Acta Pharmaceutica Sinica B 2023;13(2):517−541

Chinese Pharmaceutical Association
Institute of Materia Medica, Chinese Academy of Medical Sciences

Acta Pharmaceutica Sinica B

www.elsevier.com/locate/apsb
www.sciencedirect.com

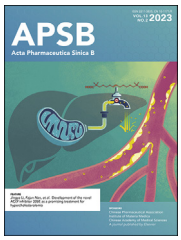

REVIEW

Medical micro- and nanomotors in the body

Huaan Li[a,b], Fei Peng[c,*], Xiaohui Yan[d,*], Chun Mao[e,*], Xing Ma[f,*], Daniela A. Wilson[g,*], Qiang He[h,*], Yingfeng Tu[a,b,*]

[a]*Department of Pharmacy, Zhujiang Hospital, Southern Medical University, Guangzhou 510280, China*
[b]*School of Pharmaceutical Science, Guangdong Provincial Key Laboratory of New Drug Screening, Southern Medical University, Guangzhou 510515, China*
[c]*School of Materials Science and Engineering, Sun Yat-Sen University, Guangzhou 510275, China*
[d]*State Key Laboratory of Molecular Vaccinology and Molecular Diagnostics & Centre for Molecular Imaging and Translational Medicine, School of Public Health, Xiamen University, Xiamen 361005, China*
[e]*National and Local Joint Engineering Research Center of Biomedical Functional Materials, School of Chemistry and Materials Science, Nanjing Normal University, Nanjing 210023, China*
[f]*Sauvage Laboratory for Smart Materials, School of Materials Science and Engineering, Harbin Institute of Technology (Shenzhen), Shenzhen 518055, China*
[g]*Institute for Molecules and Materials, Radboud University, Nijmegen, 6525 AJ, the Netherlands*
[h]*Key Laboratory of Microsystems and Microstructures Manufacturing (Ministry of Education), School of Medicine and Health, Harbin Institute of Technology, Harbin 150080, China*

Received 24 July 2022; received in revised form 24 August 2022; accepted 14 September 2022

KEY WORDS

Micro- and nanomotors;
Function integration;
Controlled propulsion;
In vivo navigation;
Biomedical applications;
Minimally invasive microsurgery;
Biosensing;
Biological barrier penetration

Abstract Attributed to the miniaturized body size and active mobility, micro- and nanomotors (MNMs) have demonstrated tremendous potential for medical applications. However, from bench to bedside, massive efforts are needed to address critical issues, such as cost-effective fabrication, on-demand integration of multiple functions, biocompatibility, biodegradability, controlled propulsion and *in vivo* navigation. Herein, we summarize the advances of biomedical MNMs reported in the past two decades, with particular emphasis on the design, fabrication, propulsion, navigation, and the abilities of biological barriers penetration, biosensing, diagnosis, minimally invasive surgery and targeted cargo delivery. Future perspectives and challenges are discussed as well. This review can lay the foundation for the future direction of medical MNMs, pushing one step forward on the road to achieving practical theranostics using MNMs.

*Corresponding authors. Fax: +86 020 62789590.
E-mail addresses: pengf26@mail.sysu.edu.cn (Fei Peng), xhyan@xmu.edu.cn (Xiaohui Yan), maochun@njnu.edu.cn (Chun Mao), maxing@hit.edu.cn (Xing Ma), d.wilson@science.ru.nl (Daniela A. Wilson), qianghe@hit.edu.cn (Qiang He), tuyingfeng1@smu.edu.cn (Yingfeng Tu).
Peer review under responsibility of Chinese Pharmaceutical Association and Institute of Materia Medica, Chinese Academy of Medical Sciences.

https://doi.org/10.1016/j.apsb.2022.10.010

1. Introduction

Nature has created sophisticated molecular motors such as myosin, kinesin and dynein[1]. These tiny machines, engineered with local fuel, function efficiently to ensure life activities in biological systems[2]. Inspired by this, scientists have invented artificial counterparts namely micro- and nanomotors (MNMs). MNMs are micro-/nanoscale devices capable of performing complex tasks in liquid media by transforming various energy sources into mechanical motion or actuation[3]. They can be propelled either by chemical fuels (*e.g.*, H_2O_2[4,5], glucose[4,6], urea[7,8], H_2O[9,10], etc.) or external physical fields (*e.g.*, magnetic[11–14] and electric field[15,16], light[17,18], ultrasound[19,20], etc.). The idea of MNMs was first envisioned by Richard Feynman in a lecture "There's plenty of room at the bottom" in 1959, where it was imagined to swallow the surgeon for the treatment of diseases[21]. Later, this fantasy emerged in science fiction movies such as the classic "Fantastic Voyage" in 1966 and the recent "Ant-Man" in 2015, which described shrunken men with small sizes to execute tasks. In fact, dreams of miniaturizing a machine come into reality due to the great advances in synthetic chemistry, material chemistry and nanotechnology. In 2002, scientists succeeded in reducing the motor size to a centimeter scale[22], followed by the birth of motors with micro/nanometer levers in 2004. Since then, the past two decades have witnessed the booming development of MNMs including fabrication approaches, motion control strategies and potential applications[3]. During this time, a large number of motors with diverse compositions (inorganic materials[23,24], polymers[25,26] or biohybrid[27–29]) and geometries (Janus sphere[30,31], tubes[32,33], rods[23,34], helix[35,36], etc.) have been widely designed and fabricated through bottom-up, top-down, or hybrid strategies. The flexibility of these fabrication techniques and diversity of compositions further facilitate the intelligentization of MNMs, which are capable of adapting to specific microenvironments[37]. As one of the most important aspects of intelligent MNMs, on-demand motion control including speed regulation and multidimensions manipulation (directional and collective behaviors[38]) is essential. Through motion control, MNMs can provide precise and active cargo transportation in different applied microenvironments, which offers great opportunities for MNMs to revolutionize the conventional biomedical field.

Medical MNMs are aiming for the diagnosis, prevention, and treatment of diseases, with the capability of executing preprogrammed medical procedures in complex biological microenvironments[39]. Apart from common characteristics of conventional passive micro- and nanoparticles, active motion behaviors offer tremendous potential for biomedical applications such as drug delivery, microsurgery, biosensing and detoxification[3,39,40]. For instance, in the field of drug delivery, active MNMs are possible to improve *in vitro* and *in vivo* performances, including cellular uptake[41,42], site-directed cell killing[43] and *in vivo* therapeutic efficacy[44,45]. Due to their mobility, medical MNMs exhibit superior functions in overcoming biological barriers such as vasculature[46], vitreous[47], mucosal[48,49] and more recently, the challenging blood–brain barrier (BBB)[50]. With these promising advances, MNMs have been considered the next generation of drug carriers in the biomedical field[51]. Besides, as miniaturized devices, MNMs are also employed as mobile therapeutic tools for minimally invasive microsurgery[47,52,53]. They can perform precise incisions with wireless control in diseased sites that are generally confined spaces, which are hard to achieve using conventional surgical procedures. Furthermore, other critical biomedical applications such as *in vivo* imaging have also been demonstrated recently[8,54]. The commonly used imaging techniques such as fluorescence, ultrasound and magnetic resonance imaging, provide great opportunities to visualize MNMs *in vivo*[40].

Despite the promising progress, challenges such as biosafety and reproducibility remain to be addressed on the way to real clinical translation. As it is still at an infancy stage, an overview of the fundamental and current progress is urgently needed. Although several detailed reviews of medical MNMs have been reported, a comprehensive summary of MNMs in biomedicine with related fundamentals is still lacking. Here, we aim to provide comprehensive perspectives of medical MNMs with emphasis on the design, propulsion and control strategies, as well as the recent advances in biomedical applications (Fig. 1). Challenges and future directions of medical MNMs are discussed as well. By summarizing the current progress, we hope that our review can lay the foundation for further development and clinical translation of medical MNMs in the future.

2. Design and fabrication of MNMs

Concerning biomedical applications, the fabrication of MNMs encounters some significant challenges due to their small size[3]. At a micro/nanoscale where Reynolds number (Re) is low, Brownian

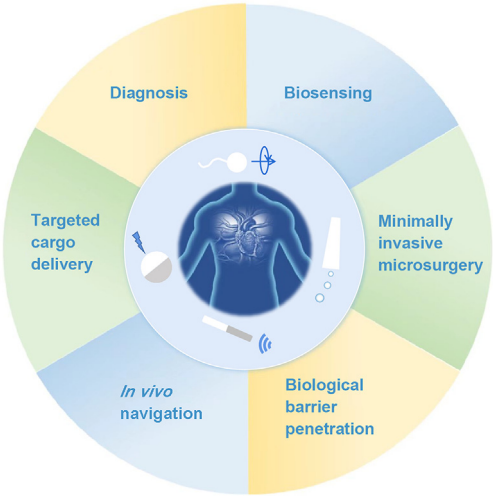

Figure 1 Medical micro- and nanomotors (MNMs) and their applications in the body.

diffusion and viscous drag dominate, significantly affecting the active motion of MNMs[55]. The viscous drag can counteract any applied forces which permit no longer continuous motion. On the other hand, Brownian diffusion generated from constant collisions between particles and surrounding solvent molecules is greatly enhanced with the decreased size of particles. To address these problems, MNMs should be designed to behave in continuous and directional motion by instantaneous forces. For that purpose, asymmetric geometry of MNMs or asymmetric distribution of actuating ingredients (*e.g.*, energy sources, reaction products) is usually needed. In this section, we summarize the design and fabrication of MNMs, along with their pros and cons.

2.1. *Deposition*

Deposition is a versatile strategy to fabricate MNMs with different morphologies and sizes. It normally allows flexible utilization of diverse materials. There are two important categories of deposition, namely physical vapor deposition (PVD) and electrochemical deposition, respectively. PVD involves the vaporization of the target materials by an electron beam or ionized argon gas, followed by the film formation on the surface of a well-arranged substrate normally a monolayer of micro- and nanoparticles[56]. Therefore, an asymmetrical structure can be realized easily through elemental deposition once released from the substrate. Different from conventional PVD (perpendicular deposition at a fixed angle onto the substrate), glancing angle deposition (GLAD), or dynamic shadowing growth enables a flexible vapor depositing angle and substrate variability, allowing for more opportunities to fabricate MNMs with diverse structures such as V-shape[57] or tadpole shape (Fig. 2A)[58]. In addition, with the deposition of physical field-responsive components (*e.g.*, magnetic materials), this technique is widely used for the fabrication of powerful MNMs that are capable of moving in complicated biological environment[59]. For instance, magnetic Ni was deposited on the spiral plant templates using electron beam evaporation, resulting in helical micromotors with powerful magnetic propulsion[60]. By using varied templates, MNMs with different shapes are easily accessible.

For electrochemical deposition, it is more convenient for a variety of scaffolds ranging from inorganic to organic materials *via* redox reactions or an external electrical current and allows the fabrication of MNMs based on the porous membrane template[56,59]. The porous membrane template is normally used as a cathode for the deposition of materials. During the process, the geometry of MNMs can be controlled simply by tuning the parameters such as the pore shape and size of the membrane template, the density of the applied current, or the electrodeposition time. For example, tubular micromotors with different lengths could be fabricated by membrane template-assisted electrodeposition with varying deposition time[61]. The obtained motors exhibited interesting length-depending motion behavior, which provides a fundamental for the fabrication of MNMs with desired moving efficiency. In addition, for biological applications, MNMs with better efficiency can be designed by applying external fields. Li et al.[62] developed a magneto-acoustic nanomotor using template-assisted electrochemical deposition followed by segment-selective chemical etching (Fig. 2B). Actuated by magnetic and acoustic fields, such hybrid nanomotors exhibited efficient motion even in blood and demonstrated attractive collective behaviors, including stable aggregation, swarm motion and swarm vortex. Another strategy termed bipolar electrodeposition is also widely used for motor fabrication. Differing from a static membrane, it involves polarized deposition of conductive materials. In the presence of an electric field, the conductive objects become bipolar electrodes, where redox reactions occur. The topology of the deposits can be controlled by adjusting the viscosity of the solution and the parameters of the applied electric field such as orientation and amplitude[63]. For instance, Fattah et al.[64] managed to fabricate two kinds of Janus carbon microobjects with different topologies based on bipolar electrodeposition. In this study, manipulating the orientation of the electric field could alter the alignment of the carbon object at a different angle, thus obtaining a centered or non-centered deposition of copper.

2.2. *Assembly*

The assembly technique has been extensively investigated for the fabrication of micro-/nanoparticles owing to the well-defined structures, flexible functionality and massive production. Assembly was first introduced in the field of MNMs in 2012[65,66]. It provides a flexible way to transform various components into uniform miniaturized structures with desired shapes and sizes. During the assembling process, catalytic engines, drugs, or imaging agents can be loaded easily, endowing the motors with multifunctionalities for various applications. There are two kinds of assembly techniques used for the fabrication of MNMs, namely self-assembly of macromolecules and layer-by-layer (LBL) assembly. The self-assembly technique involves the spontaneous reorganization of molecules into patterns and structures. Wilson and coworkers[65] reported a stomatocyte-shaped nanomotor transformed from a spherical polymersome after self-assembly of a block copolymer polystyrene-*b*-poly(ethylene glycol) (Fig. 2C). During the shape transformation, catalytic engines such as platinum nanoparticles or enzymes[67] can be encapsulated into the cavity physically. The nanocavity is access to surrounding chemical fuel for the propulsion of stomatocyte nanomotor. Moreover, one of the important advantages of using self-assembly is the flexible incorporation of smart polymers (responsive to environmental stimuli), which allows for the design of intelligent MNMs. By incorporating an atom-transfer radical polymerization (ATRP) initiator followed by brush formation of a temperature-sensitive poly(*N*-isopropyl acrylamide) (PNIPAM) polymer layer, Tu et al.[25] created a stomatocyte nanomotor capable of regulating movement *via* temperature change. The grown PNIPAM brush could function as a temperature-responsive valve to control the access of hydrogen peroxide fuel to the nanocavity of the stomatocyte, thus controlling the movement speed based on the surrounding temperature. In addition, combined smart polymers with therapeutic drugs, the assembly technique allows the fabrication of stimuli-responsive MNMs for in-site drug release. For instance, a redox-sensitive nanomotor based on amphiphilic copolymers with disulfide bridges was fabricated for anticancer drug delivery[68]. The incorporated disulfide bonds could be cleaved in the presence of glutathione which is overexpressed in the tumor microenvironment, thus achieving tumor environment-triggered drug release. In addition, the incorporation of biocompatible polymers is possible to endow medical MNMs with good biocompatibility. For instance, by self-assembly, scientists developed a series of biocompatible and biodegradable nanomotors using polymers such as poly(ethylene glycol)-*b*-polycaprolactone (PEG-*b*-PCL)[69] and poly(ethylene glycol)-*b*-poly(D,L-lactide) (PEG-*b*-PDLLA)[70,71] for nanomedicine.

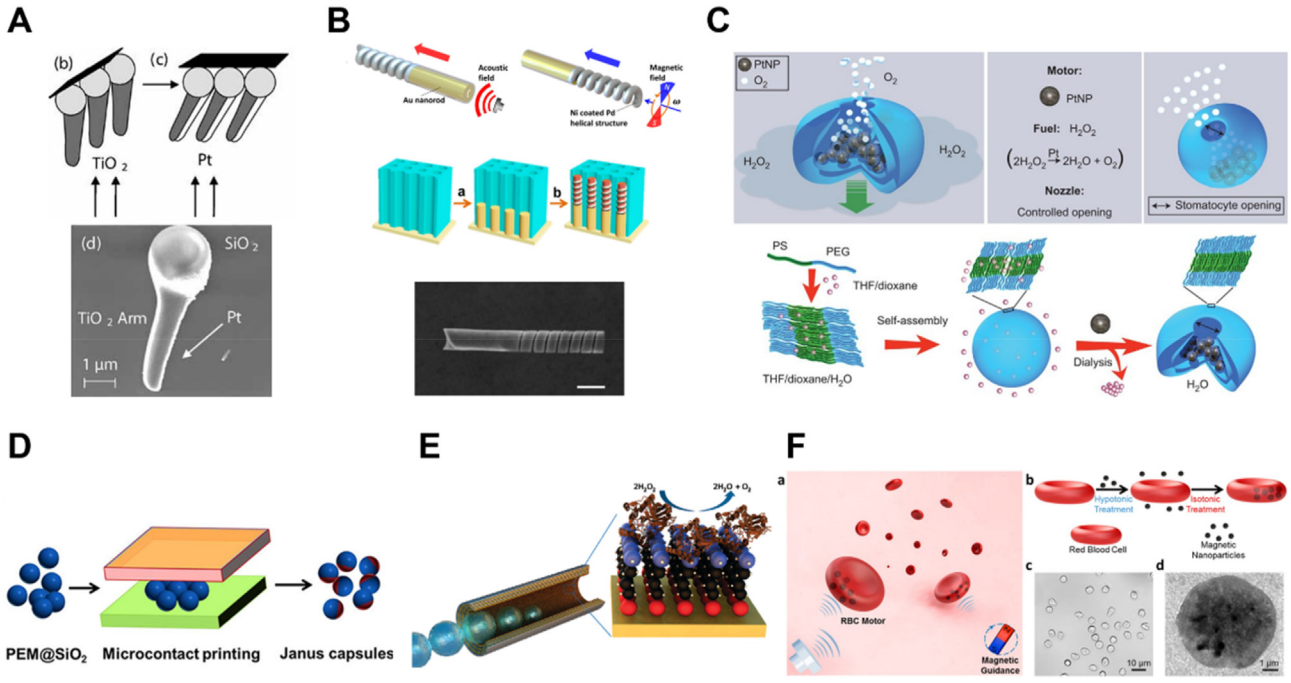

Figure 2 Design and fabrication of MNMs. (A) Fabrication of a tadpole-like nanomotor based on PVD technique. Reprinted with the permission from Ref. 58. Copyright © 2009 Wiley−VCH; (B) Preparation of a magneto-acoustic nanomotor using template-assisted electrochemical deposition followed by segment-selective chemical etching. Reprinted with the permission from Ref. 62. Copyright © 2015 American Chemical Society; (C) Fabrication of stomatocyte-shaped nanomotors using macromolecular self-assembly technique. Reprinted with the permission from Ref. 65. Copyright © 2012 Nature Publishing Group; (D) fabrication of a platinum-engined Janus capsule *via* LBL assembly. Reprinted with the permission from Ref. 66. Copyright © 2012 American Chemical Society; (E) fabrication of a tubular hybrid micromotor with catalase inside the cavity of a Ti/Au microtube. Reprinted with the permission from Ref. 77. Copyright © 2010 American Chemical Society; (F) fabrication of RBC-based biohybrid motors encapsulated with asymmetrically distributed magnetic nanoparticles. Reprinted with the permission from Ref. 81. Copyright © 2014 American Chemical Society.

LBL assembly is a common technique that applies various interactions between alternating oppositely charged materials[72]. These interactions include electronic interactions, hydrogen bonding and coordination interactions, which are widely utilized for the fabrication of various structures such as nanocapsules and nanotubes[73]. By using a variety of materials ranging from inorganic molecules, polymers, lipids and proteins to even assemblies, LBL assembly enables the flexible design of MNMs with desired shapes and sizes by altering the assembly process or the geometry of the used templates[74]. Wu et al.[66] developed a platinum-engined Janus capsule based on poly(styrene sulfonate) (PSS) and poly(-allylamine hydrochloride) (PAH) (Fig. 2D). The asymmetrically coated platinum catalysts were capable of decomposing hydrogen peroxide to propel the motor. In addition to capsule structure, tubular MNMs can also be prepared by LBL assembly. By using two natural materials namely positively charged chitosan (CHI) and negatively charged sodium alginate (ALG), the same group[75] prepared a tubular nanomotor with good biocompatibility. These polymers were absorbed into the pores of the polycarbonate template, where the platinum catalysts were asymmetrically distributed. With a conical shape beneficial for the release of oxygen bubbles produced by platinum catalyzing, this assembled nanomotor showed rocket-like behavior with a high speed of 74 μm/s. Another assembly technique based on polymer single crystals (PSC) has also been developed[76]. It relates to the assembling absorption of inorganic catalysts (*e.g.*, platinum nanoparticles) on crystalized polymers such as polycaprolactone (PCL). This strategy also allows for the asymmetric distribution of catalysts, thus enabling efficient motion. However, in terms of bioapplications such as drug delivery, micro- and nanocarriers with small sizes are preferred. Therefore, LbL assembly and macromolecular self-assembly are the better choices for the design and fabrication of medical MNMs.

2.3. *Biohybrids*

Biohybrid MNMs by integrating biological entities such as catalytic enzymes, cells, microbes, or their membranes with synthetic components have been developed as well. These combined structures exhibit excellent properties such as efficient motion, functionality and outstanding biosafety in complex physiological environments. Catalytic catalase is capable of catalyzing the decomposition of H_2O_2, which produces oxygen for motor propulsion. Sánchez's group[77] reported a tubular hybrid micromotor with catalase inside the cavity of a Ti/Au microtube. The catalase mediated the sufficient production of oxygen bubbles and drove the motor more efficiently than those platinum-engined analogs (Fig. 2E). However, high concentration of the added H_2O_2 fuel is toxic and the local H_2O_2 concentration in disease sites is low, and thus it is not an excellent choice for further biological applications. As a result, alternatives such as glucose oxidase, urease, lipase, or enzymatic cascade emerged, and they exhibited great potential for *in vivo* applications[4,7,78]. Recently, Hortelao and his coworkers[8] developed urease-powered hybrid nanomotors with

swarming behavior and achieved *in vivo* monitoring in the bladder by labeling the motor with ^{124}I and ^{18}F. Compared with nonmotile counterparts, this motor demonstrated enhanced convection and mixing in living reservoirs.

In addition to enzyme incorporation, cellular species such as sperm cells, microorganisms and blood cells are also employed for fabricating medical MNMs. A sperm cell-based biohybrid microrobot with a ferromagnetic tubular structure was first presented by Magdanz et al.[79]. In this design, the sperm cell was captured inside the microtube as an engine, while the ferromagnetic components offered remote control of motion direction. Similarly, with flagella structures for powerful propulsion, some bacteria are also considered good candidates for the construction of biohybrid motors. For example, a kind of microswimmer propelled by non-pathogenic *Escherichia coli* (*E. coli*) was developed by Stanton et al.[80]. Here, the motor was built by adhering the bacterium to metal caps of polystyrene (PS) Janus particle through the surface hydrophobicity and charges. The preferential adhesion to a specific site on the particle enabled multifunctionality of the motor towards drug delivery. However, most exotic species may suffer from immune attacks *in vivo*. Therefore, increasing efforts have been made on blood cell-based MNMs to address biocompatibility and mobility issues *in vitro* or *in vivo*. Wu and coworkers[81] designed a red blood cell (RBC)-based motor encapsulated with asymmetrically distributed magnetic nanoparticles (Fig. 2F). The asymmetry offered propelling forces under applied ultrasound, and the magnetic components provided precise guidance in the presence of an external magnetic field. With the preserved immunosuppressive property of RBCs, this biohybrid system showed efficient movement even in whole blood. Similar to intact cells, cellular components from different sources such as cell membranes can also be utilized to endow biohybrid MNMs with different types of characteristics. Wan et al.[82] reported a platelet-derived nanomotor for targeted thrombus therapy. The motor was prepared through encapsulation of the platelet membrane on the outer layer of a platinum-loaded porous nanostructure. The platelet membrane provided the ability to target the thrombus site while platinum offered near-infrared (NIR) light-driven motion capability. Upon exposure to NIR irradiation, this nanomotor loaded with thrombolytic and anticoagulant drugs, exhibited enhanced penetration and *in vivo* therapeutic effect on the thrombus.

3. Propulsion and control strategy

Since the booming development of various disciplines such as materials and nanotechnology has facilitated the design and fabrication of MNMs, the general basis of propulsive MNMs needs a better understanding and should be used to promote the on-demand design of MNMs for medical uses. In this section, we first present the principles and strategies of how to propel MNMs, including chemical propulsion and external physical field propulsion. Secondly, on the way to medical applications, we then focus on the biocompatible propulsion of MNMs under the complex biological environment which is different from that in water. As the motion in biological settings has been achieved, we intend to control their motion and provide better on-demand manipulation of MNMs. In this part, the control of speed, direction and collective behavior is discussed. Before this, the basis of motion dynamics including the calculation of speed and mean squared displacement (MSD) are provided. Finally, once MNMs are administered *in vivo*, they should be navigated to the targeted sites, which mainly relies on the real-time tracking/imaging of MNMs (individual entity or swarms) including optical imaging, ultrasound imaging, magnetic imaging, ionizing radiation-based imaging and photoacoustic imaging techniques.

3.1. General introduction of how to propel MNMs

The major difference between MNMs and conventional micro-/nanostructures is the self-propulsive ability, which offers great potential to revolutionize applications in various fields. The fundamental of MNMs construction is how to utilize energies from different environments for efficient propulsion. Based on the energy sources, the motion mechanisms of MNMs are generally classified into chemical propulsion and external physical field propulsion.

3.1.1. Chemical propulsion

Chemical propulsion normally relies on the motor's constituent materials which can catalyze the reactions with substrate fuels[73,83]. To obtain more directional and pronounced motion, chemical-driven MNMs with asymmetrical distribution of catalysts are usually designed. Based on the asymmetry structure, the substrate fuel is decomposed to yield the concentration gradient of products or generate bubbles on the catalyst side, thus propelling MNMs forward. Basically, chemical propulsion mechanisms include bubble propulsion, self-diffusiophoresis and self-electrophoresis.

Bubble propulsion emerged as the earliest type of drive and now is relatively well-developed. The chemical reactions of bubbling MNMs mainly attribute to the framework materials or the coated catalysts on the surface of the motors. The driving forces are generated once the produced bubbles detach from the motor structure, thus resulting in a continuous and rapid movement of the motor in the opposite direction (Fig. 3A)[84]. However, bubble propulsion normally requires a high concentration of chemical fuels. Moreover, the generation of massive bubbles may induce potential risks once the motors are used in the bodies.

Self-diffusiophoresis is usually caused by an asymmetric build-up of catalytic products around the motors, which results in the formation of product concentration gradients in the surrounding environment (Fig. 3B)[85]. The formed gradients start to diffuse away and further drive the motion of motors away from the catalyst. Normally there are two kinds of diffusiophoresis namely electrolyte and non-electrolyte diffusiophoresis[86]. Non-electrolyte diffusiophoresis refers to the formation of nonionic gradients, whereas electrolyte diffusiophoresis involves the ionic species that diffuse with different speeds and induce a temporary electric field around the motor particles. Compared with bubble propulsion, MNMs based on self-diffusiophoresis normally move at a lower rate[87].

Different from self-diffusiophoresis, self-electrophoresis is normally attributed to the asymmetric distribution of ionic products around the motors, which generates a local electric field (Fig. 3C)[88]. The generated electric field induces an electrophoretic effect, therefore, the charged MNMs move through the electric field or generate mutual aggregation and repulsion behaviors. MNMs based on self-electrophoresis act as self-contained electrochemical cells, where oxidation and reduction reactions occur at the anode and cathode of MNMs, respectively[89]. Paxton et al.[90] fabricated Pt/Au bimetallic nanorods by electrochemical methods, in which Pt catalyzed the decomposition of H_2O_2. The catalytic

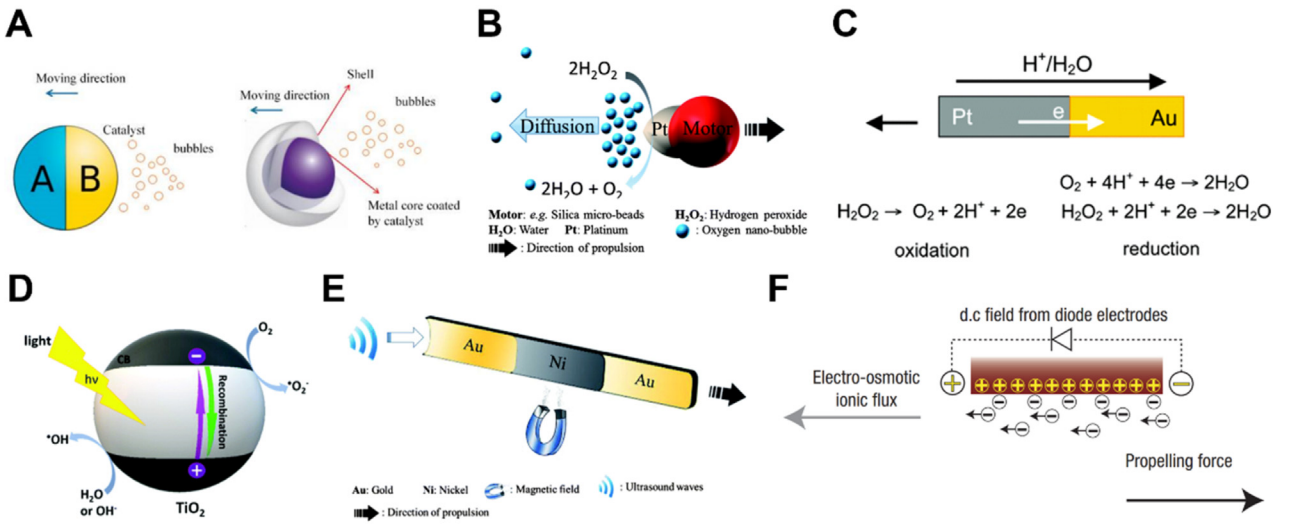

Figure 3 Propulsion strategies of MNMs. (A) Bubble propulsion of MNMs. Reprinted with the permission from Ref. 84. Copyright © 2018 Multidisciplinary Digital Publishing Institute; (B) self-diffusiophoresis of MNMs. Reprinted with the permission from Ref. 85. Copyright © 2014 The Royal Society of Chemistry; (C) Self-electrophoresis of MNMs. Reprinted with the permission from Ref. 88. Copyright © 2006 American Chemical Society; (D) light-driven MNMs. Reprinted with the permission from Ref. 93. Copyright © 2019 The Royal Society of Chemistry; (E) magnetic field-driven MNMs. Reprinted with the permission from Ref. 85. Copyright © 2014 The Royal Society of Chemistry; (F) electric field-driven MNMs. Reprinted with the permission from Ref. 99. Copyright © 2007 Nature Publishing Group.

reaction resulted in a net flow of electrons from Pt to Au end and simultaneous protons' migration to Au side. Therefore, the negatively charged nanorods moved toward the proton-rich region. However, high ion concentrations in the bodies can severely quench the electrophoretic process, resulting in limited motion capability of self-diffusiophoretic MNMs *in vivo*.

3.1.2. *External field propulsion*

External physical fields such as light, magnetic, electric and ultrasonic fields can also be used for the actuation of MNMs. Different from chemical propulsion, it relies on energy input from an external field to obtain kinetic driving force, which can effectively avoid the limitation of chemical fuels. For light-driven MNMs, it usually requires the introduction of photoactive components into the structures[18,91]. Photoactive materials can absorb light energy and in turn trigger the photocatalytic reaction[92], photothermal effect[93], or photochromic transformation[94], thus generating asymmetric fields around or in the MNMs to achieve autonomous movement (Fig. 3D). Moreover, by changing the intensity or lighting direction of the applied light, both velocity and direction of motors can be manipulated especially for photocatalytic motors[94]. One typical light-driven motor is TiO_2-based micromotor, in which photoactive TiO_2 undergoes photocatalytic reactions upon light irradiation. Under UV light, the TiO_2 side of the developed SiO_2−TiO_2 Janus motors could induce the formation of chemical species (*e.g.*, ·OH, H^+) and the diffusion of these species led to the motion of the motors[95].

Magnetic field has been widely used for MNMs propulsion because of its noninvasiveness and superior controllability[96]. Generally, magnetic components need to be incorporated into the motor system to achieve magnetic responsiveness under the magnetic field (Fig. 3E)[85]. Zhang et al.[97] fabricated a multilayer metallic helical nanosheet composed of Cr/Ni/Au. The resulting motors could be controlled under a low-intensity rotating magnetic field with a speed of over 12 μm/s, which is comparable with natural microorganisms. In the presence of a rotating magnetic field, these kinds of helical magnetic MNMs are possible to rotate along the axis of the helix to produce translational motion[98]. In addition to magnetic field, electric field, as a kind of clean, economical and practical energy source, can also be used for the propulsion of conductive MNMs (Fig. 3F)[99]. The motion behavior of MNMs can be regulated either by tuning the surface charge of the motor itself or modulating the interfacial electrochemical reaction. Through manipulating the geometries and the direction of the electric field, the motion of MNMs can be controlled as well[99]. For instance, under asymmetric electrofluid conditions, active colloids with varied compositions and shapes showed different moving patterns including translation, rotation and circulation[100]. As an acoustic wave with a frequency of over 20,000 Hz, ultrasound exhibits good directionality, strong penetration ability and outstanding biocompatibility, which is used as a common energy source for the propulsion of MNMs. Ultrasound-propelled MNMs normally include soft microcontainers driven by oscillating trapped bubbles, and nonresonating bimetallic nanowires propelled by scattering of acoustic waves[101]. With tunable acoustic parameters (*e.g.*, frequency, voltage), these motors usually demonstrate powerful propulsion. For example, ultrasound can drive metallic microrods at a speed of up to 200 μm/s[34].

3.2. *Biocompatible propulsion within biological environment*

From the initial movement in an aqueous phase to PBS solution, then to simulated body fluid, and finally, to complex biological settings including *in vitro* serum or blood, and even real human environments, the motion capability of MNMs in complex physiological environments has attracted more and more attentions[102,103]. However, biocompatible propulsion of medical MNMs is normally neglected. For many chemical-driven motors reported before 2019, high concentrations of H_2O_2 (2%−20%) were usually used, which are toxic to cells and organisms[75,104].

MNMs designed in this way cannot be used in biomedical applications. Therefore, the biocompatible propulsion of MNMs in the bodies is of great significance.

Medical MNMs face complicated physiological environments that contain a high concentration of ions, specific pH in different locations, various proteins and considerable fluid viscosity[105]. A high ion concentration, for example, can severely impair the mobility of motors especially driven by self-electrophoresis[3]. As a result, it is of great importance to improve the ion tolerance of MNMs in such media. Recently, a polymer coating was incorporated on the surface of motors and served as the primary ion conductive channel to prevent the quenching of the electrophoretic process[106]. In another example, high ion tolerance of poly(-heptazine imide) (PHI) carbon nitride-based light-driven microswimmers was achieved by the interplay between PHI's textural and structural porosity, and the optoionic effects which facilitate ion traveling into and through the particle[107]. Meanwhile, protein corona can be easily formed once the motors enter the blood, resulting in limited performance in biological environments[40]. This means the antifouling modification of the motor surface is necessary. Other strategies such as the utilization of external physical fields can also be considered to reduce the influence of physiological environments. The external energy sources, especially magnetic field, ultrasound, and light provide excellent driving forces with wireless manipulation. For instance, NIR light is commonly used to drive MNMs. And the motion speed of these MNMs depends on the irradiation power of the NIR light source. However, due to the photothermal effect, great damage to normal tissues may happen if the intensity of the applied NIR is too high[108]. Therefore, guaranteeing efficient motion of MNMs *in vivo* with suitable light intensity needs to be considered. Meanwhile, the concomitant photothermal effect can also be utilized for potential photothermal therapy. In terms of magnetic MNMs, no obvious biological harmfulness has been reported in previous studies. Compared with optical ones, magnetic field-driven MNMs have better controllability and stronger penetration ability[109,110], thus providing an active and precise motion towards the target in the bodies. However, there are also some defects, for example, the need for complex magnetic field design[109].

In view of chemical-driven MNMs, despite producing wastes (such as carbon dioxide, magnesium hydroxide, etc.) that are not beneficial to the bodies during self-propelled process[110], the flexible choices of materials and easy propulsion procedures without external equipment still offer promising practical uses in biomedicine. Therefore, the design of chemical MNMs that can adapt to the living environment has also become the frontier focus of research in this field. For example, magnesium-based micromotors only rely on water to generate driving force through the detachment of hydrogen (H_2) bubbles. Based on the reducibility of the produced H_2, active H_2 therapy towards acute ischemic stroke[111] and rheumatoid arthritis[10] was achieved by using the produced products during motion. In addition, the enzyme-triggered biocatalytic reaction usually occurs in a relatively mild physiological environment with higher efficiency than the artificial one. By decomposing endogenous fuels especially those related to diseases, enzymatic MNMs can not only realize biocompatible propulsion in the bodies but also achieve active therapy by clearing those disease markers. Another strategy is to utilize the endogenous reaction *in vivo* to drive MNMs. Wan et al. proposed to fabricate nitric oxide (NO)-driven nanomotor[112] and hydrogen sulfide (H_2S)-driven nanomotor[113], based on endogenous reactions for cancer therapy in an animal model, which promoted *in vivo* applications of biomedical MNMs.

3.3. Motion dynamics

In principle, the motion dynamics (or mobility) of MNMs can be characterized by speed and diffusivity. The speed calculation is usually helpful for MNMs with a specific moving pattern (*e.g.*, ballistic directional motion), while the diffusivity analysis is preferred for nano-sized motors with enhanced diffusion. To obtain these two parameters, particle tracking is needed, and generally, it can be recorded by optical microscopy or light scattering technique. The experimental and calculation procedures have been introduced previously[114–116] and were elaborated recently in a corresponding guide initiated by Wang et al.[117].

Generally, for motors with large sizes (>1 μm), the calculation of instantaneous speed is carried out to evaluate the mobility[117]. First, the moving trajectories (including the x and y coordinates) can be acquired by optical microscopy and then plotted as a function of time. Second, in this plot, the displacement can be divided by the time interval (Δt), yielding the instantaneous speed of the particle. By doing this, one can also calculate the average speed of the particle during its moving process and more importantly, analyze a large number of particles to assess their mobility.

For motors in nanoscales, a more appropriate way to quantity the moving dynamics is the calculation of MSD[114,115]. MSD refers to the position change of a particle over time. The speed and the diffusion coefficient can be also exacted from MSD. Typically, there are two situations. At shorter time intervals (Δt), where the motor particle seems to continuously move in a specific direction, MSD can be calculated from Eq. (1):

$$\mathrm{MSD}\,(\Delta t) = 4D_t\Delta t + v^2\Delta t^2, (\Delta t \ll \tau_r) \tag{1}$$

where v is the speed, D_t and τ_r are the translational diffusion coefficient and rotational diffusion time respectively. Eq. (1) usually displays a ballistic curve from the motor with a propulsive or ballistic moving trajectory. On the other hand, over longer time intervals (Δt), where the motor particle seems to display enhanced or effective diffusion, MSD can be obtained from Eq. (2):

$$\mathrm{MSD}\,(\Delta t) = \left(4D_t + v^2\tau_r\right)\Delta t = 4D_e\Delta t\,, (\Delta t \gg \tau_r) \tag{2}$$

where D_e represents the effective diffusion coefficient. This is normally defined as the linear regime.

MSD can be also acquired from optical tracking, dynamic light scattering (DLS), or nanoparticle-tracking analysis (NTA)[114]. As mentioned above, using optical tracking, one can record the location of the motor and plot the displacement (MSD) as a function of time, followed by the analysis of MSD using the equations. However, due to the resolution limit of optical instruments (~200 nm), this technique is usually favored for MNMs larger than 200 nm. On the other hand, DLS has a better resolution for nano-scaled particles and thus is more suitable for sub-micrometer particles. Through DLS, one can analyze a large population of particles and obtain the diffusion coefficient without tedious calculation procedures. In recent years, NTA, similar to DLS using the light scattering technique, has emerged as an effective tool for the dynamic analysis of sub-micrometer motors. It has an additional function of particle tracking to overcome the deficiency of DLS such as the identification of aggregates.

However, it's worth noting that to get a reliable result, one should be very careful with the procedures of the measurement

and MSD analysis[117]. In particular, one should note the drifting phenomenon of MNMs while tacking their trajectories. This probably occurs when all the MNMs move in the same direction in the observed view, which also yields a misinterpreted parabolic MSD curve. The reasons may come from all kinds of aspects, such as the containment in the solvent, the arising bubbles, or the uneven instrument stage[117]. To address the drift, one should be very careful while performing these experimental procedures, strictly follow the operation guidelines, and importantly introduce the control experiments. Other solutions include using the microfluidic channels with confined space[118], or correcting the original tracking data by software/codes[117].

3.4. *How to control motion direction and behavior*

As MNMs have attracted more and more attention, the control of their motion has always been a hot topic. Typically, the motion direction refers to the individual moving direction of each MNM particle, while the behavior indicates the collective behavior of MNM clusters. The collective behavior includes swarming, schooling, excluding, etc., which resembles the behavior of microorganisms in nature. To accomplish on-demand tasks, reliable control of the motion trajectories and motion behaviors of MNMs is necessary and also important in a practical sense. The direction and the collective behavior can be controlled by tuning the parameters of the applied external field or the chemical substrates, according to MNMs driven by different sources.

For chemical fuel-driven MNMs, changing the motion environment normally affects the propulsive efficiency of the motors. Typically, the motors' speed increases with the increasement of fuel concentration, which is dominated by regulating the catalytic reaction rate[119]. For instance, Wilson et al.[120] revealed the dependence of the velocity on fuel concentration for the supramolecular catalytic nanomotors. Besides, by adding chemical inhibitors (Ag^{+}/Hg^{2+}) and a reactivator (DTT) to regulate the catalytic activity of enzymes, Ma and coworkers[7] realized precise control over the speed of urease-powered micromotors. Because directional movement is necessary for many applications such as targeted drug delivery, magnetic materials were incorporated for motion guidance of the previous urease motor under an external magnetic field (Fig. 4A).

For external field-actuated MNMs, the motion direction and behavior can be controlled by the external energy fields flexibly[121−123]. For example, by precisely regulating the strength of the energy output and the direction of the physical fields, the speed and the directionality of the motors can be simply manipulated. Among the external physical fields, magnetic fields are most widely used to guide the behavior of magnetic MNMs. Their motion trajectories can be controlled by modulating the magnetic torque and magnetization direction of the magnetic field. Lin et al.[124] developed a magnetically actuated peanut-shaped hematite colloid motor with different motion behaviors in a fluid by manipulating an external magnetic field. The peanut motor moved in a rolling mode under a rotating magnetic field, which could achieve precise motion in a pre-designed trajectory; and under a conical rotating magnetic field, the motor could climb over steep slopes in a wobbling mode to move in much more complex surroundings. Through a combination of rolling and wobbling movements, these peanut motors could autonomously transport and release cells to a pre-defined position (Fig. 4B). In addition, the motion behavior of MNMs can also be controlled by light and ultrasonic fields. For example, Xuan et al.[121] reported that the "on/off" motion and the swing behavior of the carbonaceous nanobottle (CNB) motors could be modulated by adjusting the NIR light source (Fig. 4C).

The direction of MNMs can also be controlled by the biomimic property of taxis, meaning the MNMs can move towards (positive) or away from (negative) a source such as light and chemical substrates[125,126]. Chen's group[123] reported isotropic semiconductor-based MNMs with bio-mimic phototaxis. By adjusting the direction of the incident light and photoresponsive properties of the used semiconductors, the bio-mimic behaviors of positive or negative phototaxis were observed due to the photoinduced reactions on the surface of the motors. Inspired by the phototaxis of microorganisms in nature, Dai et al.[17] synthesized a Janus nano-tree swimmer that could "turn" along the lighting direction, and they successfully programmed both positive and negative phototaxis swimmer through chemical modification (Fig. 4D). In addition to light, there are also some reports using chemical signals (such as substance concentration gradient) to guide the movement of MNMs[104,127]. Recently, positive chemotaxis of Janus or flask-like glucose-fueled motors along the glucose concentration gradient has been reported[128,129]. Dey et al.[130] demonstrated the pH taxis of an intelligent catalytic microswimmer. When the micromotors were placed in a dilute H_2O_2 bath with a pH gradient, the intelligent motor was able to sense the pH gradient and move towards a higher pH region at a faster rate. Baraban and coworkers[125] also found the chemotaxis of catalytic motors including tubular microjets and Janus particles to high concentrations of hydrogen peroxide in a microfluidic system. Exploiting the chemotaxis of catalytic motors sensitive to the hydrogen peroxide signal, scientists[26,104] reported that supramolecular nanomotors loaded with cargo were autonomously directed to specific cellular or inflammatory tissue. In addition, Shao's team[126] integrated living cells with intrinsic chemotaxis (such as neutrophils) to synthesize self-guiding hybrid micromotors for targeted drug delivery.

Apart from the individual motion of each MNM particle, collective behaviors of MNM clusters are also commonly observed. Inspired by nature, collective behaviors like swarming and assembling can carry out complex and cooperative functions that cannot be accomplished individually. Therefore, controlling the collective behavior of MNMs to simulate the aggregation/separation of biological systems is one of the current research interests[131]. In recent years, researchers have developed various strategies to realize programmable self-assembly and dynamic swarming of colloidal particles by using different stimuli, such as chemical gradients[132,133] and external energy fields (such as ultrasonic, electric, magnetic field or their combination)[134−136], which can be reconfigured into multiple forms to perform different grasping or motion tasks. A chemical gradient is possible to induce the collective behavior of MNMs. For instance, Duan et al.[132] showed that the Ag_3PO_4 micromotors could realize the transition between the "exclusion" and "schooling" behaviors with the addition or removal of NH_3 or in response to UV light, because of the change of chemical equilibrium in the colloidal particle system (Fig. 4E). In addition, applying ultrasound to MNMs can also control the collective behaviors. It was reported that the use of ultrasonic fields could control the migration of Pt−Au nanowire motor swarms[137]. Because the ultrasound could produce many pressure nodes, which could drive the colloidal particles to aggregate and move along the pressure gradient. Besides, alternating current electric fields can also manipulate collective behavior. It can induce the aggregations of MNMs, resulting in the

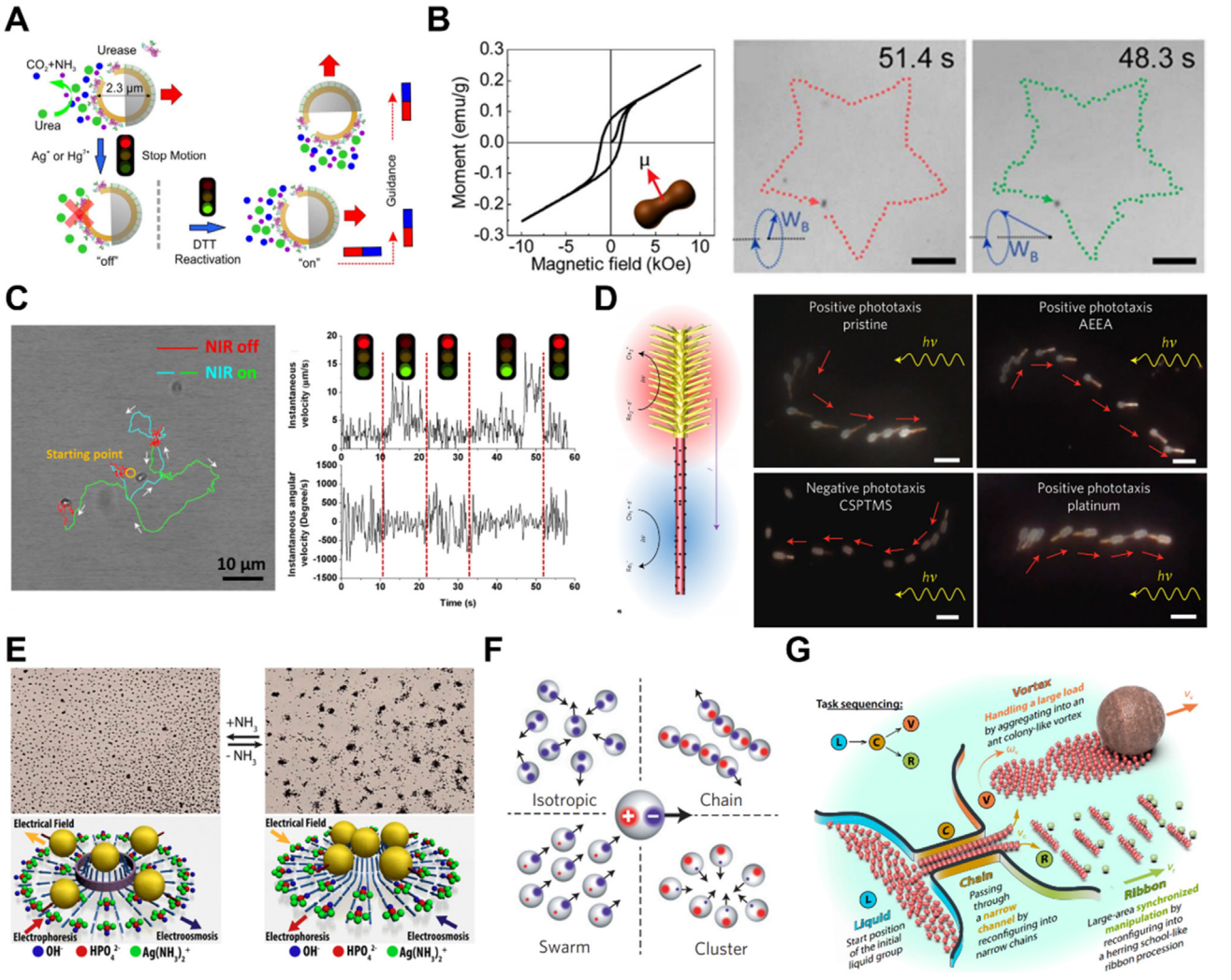

Figure 4 Control on the motion direction and motion behavior of MNMs. (A) Motion control of enzyme-driven motor by chemical addition and magnetic fields. Reprinted with the permission from Ref. 7. Copyright © 2016 American Chemical Society; (B) controlled motion pattern and trajectory of the peanut motor under magnetic field. Reprinted with the permission from Ref. 124. Copyright © 2018 American Chemical Society; (C) motion behavior of CNB motor controlled by NIR light. Reprinted with the permission from Ref. 121. Copyright © 2018 Wiley−VCH; (D) positive and negative phototaxis of artificial nanotree programmed by chemical modification. Reprinted with the permission from Ref. 17. Copyright © 2016 Nature Publishing Group; (E) exclusion and schooling behaviors of Ag_3PO_4 microparticles by adding or removing NH_3. Reprinted with the permission from Ref. 132. Copyright © 2013 American Chemical Society; (F) formation of different collective states by the spheres with imbalanced, off-centered charges that triggered by an electric field. Reprinted with the permission from Ref. 138. Copyright © 2016 Nature Publishing Group; (G) collective manipulation of micro-robotic swarms for completing the tasks. Reprinted with the permission from Ref. 109. Copyright © 2019 American Association for the Advancement of Science.

formation of chains, clusters, swarms and other patterns according to the output frequency of the applied electric field (Fig. 4F)[138]. Similarly, stimulated by an external magnetic field, the microswimmers can also exhibit a variety of interesting collective behaviors. The strategy of using oscillating magnetic fields to generate a ribbon-like paramagnetic nanoparticle swarm was reported by Yu's team[139]. By adjusting the input domain, the particle swarms could perform reversible elongation of the ribbon, as well as splitting and merging behaviors. Under the control of an oscillating magnetic field, colloidal microswarms were able to move stably through a restricted channel network and towards multiple targets. Xie et al.[109] used alternating magnetic fields to program hematite colloidal particles into four formations, including liquid, chain, vortex and ribbon microrobot swarms, respectively. Transformations among these swarms were controlled by manipulating the magnetic moment. More importantly, these reconfigurable swarms of microrobots can provide multiple collective behaviors that are responsive to changing environments and meet multitasking demands. For instance, the swarms of motors can realize functions, such as passing through a confined channel by reconfiguring into narrow chains, carrying loads by reconfiguring into ant colony-like vortices and realizing large-area synchronized manipulation by forming a herring school-like ribbon (Fig. 4G). Ahmed et al.[122] reported that magnetic particles tend to form linear chains under rotating magnetic fields with low intensity. With increasing intensity of the magnetic field, these chains disassembled and evolved into swarms. Moreover, some researchers used hybrid fields to control the motion

behavior of MNMs. Li's group[62] reported a hybrid nanomotor that exhibited diverse biomimetic collective behaviors, including stable aggregation, swarm motion and swarm vortex, in response to different field inputs. And Zhou et al.[140] combined light and ultrasonic fields to control the aggregation/separation of artificial nanomotors. It was shown that the nanomotors gathered at pressure nodes in the ultrasonic field, and displayed a collective "fireworks" separation behavior under light illumination.

3.5. *In vivo imaging and navigation*

The flexible and controllable motion of MNMs in medium provides promising potential for performing precise and complex tasks *in vivo*. However, to ensure the function of MNMs *in vivo*, it is essential to visualize the position or the locomotion of individual MNM particles or MNM clusters. First of all, once MNMs are administered *in vivo*, how to navigate them to the target sites remains to be addressed. One feasible strategy is to use innate taxis, which can achieve autonomous control. This was demonstrated by engineered bacterial MNMs. Alternative approaches include path planning and visual feedback control, both of which can be applied to almost all existing MNMs. The navigation accuracy of MNMs mainly relies on imaging-based *in vivo* tracking, especially real-time tracking. To date, many imaging techniques have been reported for the visualization of MNM swarms or individual entities, and their surrounding physiological environments. This section discusses several favorable imaging techniques of *in vivo* tracking in terms of optical imaging, ultrasound imaging, magnetic imaging, radionuclide imaging and photoacoustic imaging.

3.5.1. *Optical imaging*

Optical imaging demonstrated herein includes optical microscopy imaging, optical coherence tomography (OCT), fluorescence imaging (FL) and catheter camera-based imaging. By applying a visible light source, optical microscopy imaging has the advantage of high spatial/temporal resolution. Bergeles et al.[141] developed an electromagnetic control system suitable for small animal attempts, which was able to localize the microrobotic device using the aid of a matched algorithm. More importantly, optical imaging has a high imaging speed, which is good for locomotion tracking. For instance, Ullrich et al.[142] also integrated the microrobotic systems with a surgical microscope and achieved the real-time tracking of microrobot locomotion in porcine/lapine eyes. The camera mounted on the microscope could acquire consecutive images at a speed of 15 Hz, and the noise of the microrobot position was filtered by a moving average filter with a window size of 10 data points (Fig. 5A). However, the scattering and low penetration depth of light are still challenging.

OCT is an interferometric technique that utilizes the short coherence length of a light source to record coherent gated images and obtain cross-sectional information, which is good for MNMs navigating and tracking in tissues with high resolution[143,144]. With the aid of OCT, Li's team[145] investigated the tracking and navigation of magnetically-driven micromotors in a mouse portal vein with a high scanning rate (5.5−70 kHz) and resolution (Fig. 5B). The OCT was also applied as a non-invasive method to monitor the long-distance intravitreal movement of a swarm of helical propellers in the eye[47]. These works demonstrated the possibility of OCT imaging for potential clinical applications. However, the high acquisition time of OCT results in an insufficient ability for real-time imaging.

FL imaging has been extensively explored in the biomedical fields and can acquire continuous images at high resolution within a short time, and it has almost no damage to living organisms, providing an effective and biocompatible way for *in vivo* navigating and tracking of MNMs. Servant et al.[146] developed an isothiocyanate dye-labeled artificial bacterial flagella (ABFs). The dye features an excitation wavelength of 745 nm and an emission wavelength of 810−875 nm, where biomolecules exhibit low absorption in this emission region. After injection, the ABFs actuated by magnetic fields could be observed, tracked and navigated under the FL imaging (Fig. 5C). Apart from fluorescence dyes, natural pigments such as chlorophyll in cyanobacterial cells were also harnessed for FL imaging. In this domain, Yan et al.[147] fabricated multifunctional biohybrid magnetite microrobots from *Spirulina platensis* by a facile dip-coating in Fe_3O_4 nanoparticles suspension and made full use of the autofluorescence of the *Spirulina* for FL imaging. Under a magnetic field, the microrobots could approach the designated sites which could be tracked by FL imaging in the intraperitoneal cavity of mice. However, FL imaging remains several challenges, such as the instability of fluorescence dyes for constant tracking and its weak ability for deep tissue penetration.

Catheter camera-based optical imaging is commonly used for the diagnosis and treatment of major diseases in the gastrointestinal tract, bladder, uterus, etc., which offers good tracking ability of MNMs in deep tissues or organs. More importantly, it enables real-time localization and tracking of MNMs in an interventional manner. Wang and coworkers[148] developed an integrated platform, referred to as endoscopy-assisted magnetic actuation with a dual imaging system (EMADIS). The precise delivery of magnetic soft stem microrobots into the bile duct was achieved using this system (Fig. 5D). Although catheter-based techniques can be effective, they have low compliance and limited applications due to their inability to reach tiny blood vessels or organs.

3.5.2. *Ultrasound imaging (USI)*

B-mode ultrasound imaging was successfully demonstrated for MNMs navigating and swarm tracking, which could enhance the MNM number and imaging contrast in local areas. Yu et al.[149] demonstrated the B-mode imaging-guided navigation of a rotating colloidal swarm consisting of MNMs that feature periodic contrast changes. Subsequently, *ex vivo* localization of magnetic swarms was also accomplished by the same group[134] in bovine eyeballs and swine bladders (Fig. 5E). Ultrasound images can also be produced with Doppler imaging technique through the traveling frequency shift caused by an interaction between ultrasound waves and moving objects, desired for MNMs tracking. In a previous study, Singh and coworkers[150] reported color Doppler imaging enabled the *ex vivo* tracking of mobile paramagnetic hairbots under a chicken breast (Fig. 5F). Nevertheless, USI needs to improve its resolution at the micro/nanoscale. USI has other shortcomings, such as positioning errors, artifacts and unsatisfied background signals, and it is not suitable for imaging gas-containing organs due to the obstruction caused by gas and bone.

3.5.3. *Magnetic imaging*

As a traditional way to investigate the anatomy and physiology of the bodies, magnetic imaging is a suitable technique for *in vivo* tracking of MNMs. On one hand, it has excellent signal intensity and image quality. On the other hand, it demonstrates higher penetration depth compared with fluorescence-based imaging. Technological breakthroughs have been made by Benoit and

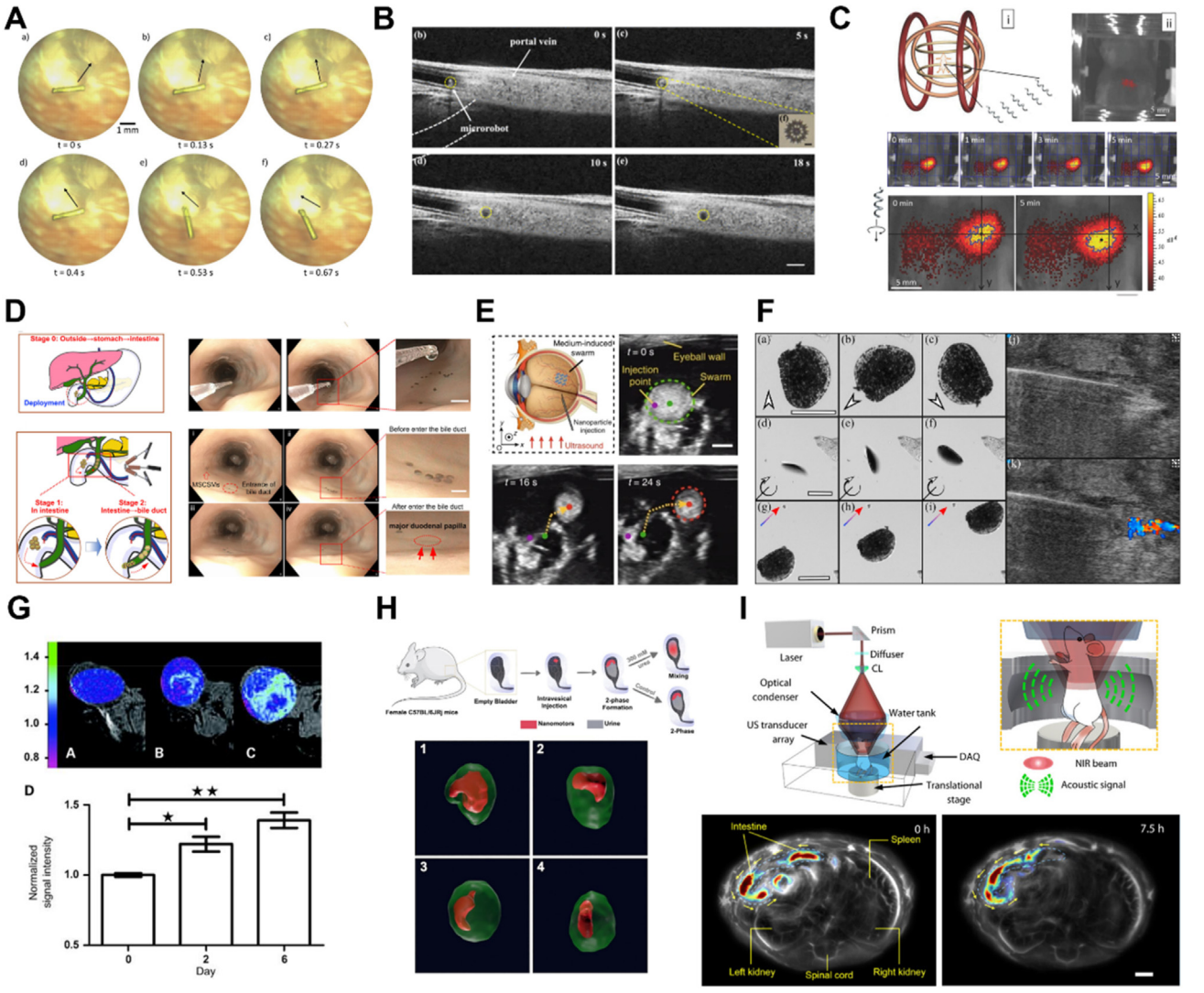

Figure 5 *In vivo* navigation of MNMs. (A) Microrobot in lapine vitreous tracked by microscopy. Reprinted with the permission from Ref. 142. Copyright © 2013 The Association for Research in Vision and Ophthalmology; (B) tracking and navigation of magnetically-driven micromotors in a mouse portal vein by OCT. Reprinted with the permission from Ref. 145. Copyright © 2019 IEEE; (C) navigation of a swarm of ABFs in the intraperitoneal cavity using FL imaging. Reprinted with the permission from Ref. 146. Copyright © 2015 Wiley−VCH; (D) rapid delivery of MNMs to the bile duct *via* a natural orifice under the navigation of endoscopy. Reprinted with the permission from Ref. 148. Copyright © 2021 American Association for the Advancement of Science; (E) USI for tracking of a swarm of MNMs in the bovine eyeball. Reprinted with the permission from Ref. 134. Copyright © 2019 Nature Publishing Group; (F) the tracking of mobile hairbots under color Doppler imaging in a chicken breast *ex vivo*. Reprinted with the permission from Ref. 150. Copyright © 2019 Elsevier; (G) biohybrid magnetotactic micromotors capable of colonizing mouse tumor xenografts and producing positive MRI contrast. Reprinted with the permission from Ref. 151. Copyright © 2009 American Association for Cancer Research; (H) PET-CT analysis of ^{18}F-nanomotors biodistribution in the bladder. Reprinted with the permission from Ref. 8. Copyright © 2021 American Association for the Advancement of Science; (I) time-lapse PAI images of MNMs in intestines for 7.5 h. Reprinted with the permission from Ref. 54. Copyright © 2019 American Association for the Advancement of Science.

coworkers[151]. They harnessed magnetotactic bacteria into biohybrid micromotors being able to colonize mouse tumor xenografts and produce positive MRI contrast, providing a potential tool for improving MRI visualization of cancer (Fig. 5G). As a promising cancer imaging technology, magnetic particle imaging (MPI) has a high contrast (no tissue background signal), high sensitivity, and infinite imaging regions throughout the body. The MPI is also a powerful tool for imaging-guided actuation of MNMs because of its high-intensity field gradients and fast localization[152−154]. Nevertheless, it is still difficult to translate this technology into *in vivo* scenarios. On one hand, a balance must be struck between scaling up the platforms to enable human-sized workspaces and maintaining high imaging quality. On the other hand, the MPI cannot capture biological tissues, resulting in an inaccurate view of the surroundings of MNMs.

3.5.4. *Ionizing radiation-based imaging*

Ionizing radiation-based imaging, such as X-ray imaging and radionuclide imaging, with deep tissue penetration and high spatial resolution[155], is a fantastic tool for *in vivo* MNM navigation and tracking. In 2018, a real-time position and navigation platform built on a principal component analysis algorithm

implemented on X-ray imaging was proposed for tracking a millimeter-sized intravascular robot *in vitro*[156]. Later, the same group presented that the platform could be used in treating arterial thromboembolism with a magnetic robot penetrating a blood clot under X-ray imaging-guided control[157]. However, it should be always noted that excessive X-ray exposure can cause side effects.

Radionuclide imaging is usually referred to as positron emission tomography (PET) and single-photon emission computed tomography (SPECT). With γ-ray emitted from radioisotopes (SPECT) and the interaction of positrons and electrons (PET), 3D images of the targeted area can be captured. The ability of γ-ray to penetrate tissue makes it effective for the navigation of MNMs *in vivo*. Vilela and coworkers[158] reported the combination of CT and PET for the tracking of a swarm of tubular Au/PEDOT/Pt micromotors. In this study, PET tracking was enabled with 7 frames over 15 min due to the absorption of ^{124}I on the micromotor surface. Following this, they employed a combination of optical microscopy and PET/CT imaging to investigate the collective behavior of enzymatic nanomotors labeled with ^{124}I and ^{18}F *in vitro* and *in vivo*[8]. The results demonstrated PET/CT imaging was highly useful for tracking nanomotor swarms *in vivo* (Fig. 5H). SPECT imaging is not currently used for tracking of MNMs but has been used for millirobots. For instance, Iacovacci et al.[159] reported a soft hydrogel-based thermo-responsive millirobot labeled with ^{99m}Tc for targeted drug delivery in the peritoneal cavity of a mouse under the monitor of SPECT imaging.

3.5.5. *Photoacoustic imaging (PAI)*

PAI, with optical contrast and acoustic resolution, is a non-invasive way for *in vivo* navigation and real-time tracking of MNMs. Aziz and coworkers[160] reported for the first time the real-time tracking of individual MNM in *ex vivo* chicken breast and scattering phantom at the depth of 1 cm. The MNM reported here was coated with Au nanorods for enhancement of the PAI signal to distinguish it from the surrounding tissue easier. Similarly, Wu et al.[54] developed Au layer-coated MNMs for PAI navigation in the intestine. MNM-based capsules could be tracked with PAI at a depth of 7 cm below the surface of the tissue. Additionally, PAI was used to observe the locomotion of MNMs toward a colon tumor, indicating the possibility of imaging-guided cancer therapy (Fig. 5I). Owing to the excellent photoacoustic effect of polydopamine (PDA) coating, magnetic *Spirulina* microrobots coated with PDA could be tracked by PAI to show their accumulation in the skin, providing further diagnosis and photothermal treatment of pathogenic bacterial infections[161]. Besides, enzyme-powered liquid metal MNMs coated with PDA also enabled real-time PAI tracking in the bladder of mice[162]. Moreover, Zhong et al.[163] recently proposed a cancer therapy platform based on magnetically engineered *Spirulina* microrobots. In this study, PAI was employed to monitor the accumulation of microrobots in tumors. Given that the optical attenuation and the ultrasonic propagation are susceptible to the influence of air, PAI imaging has its limitations, limited imaging depth remains challenging for PAI imaging.

4. Biological applications of MNMs

4.1. *Biological barrier penetration*

Although plentiful progress of MNMs in design, fabrication, navigation and imaging has been achieved, to enter the body for medical applications, MNMs still face various biological barriers such as hemorheological barrier, protein corona, BBB, mucus barrier, vitreous barrier and cell membrane barrier. If MNMs do not penetrate or overcome these biological barriers, in this case, there will be no difference between active MNMs and passive nanoparticles. Therefore, how to penetrate the biological barriers is a key issue of the medical MNMs in the bodies. Basically, the anti-biofouling structure modification, cell-based chemotaxis property and the employment of powerful external physical fields, etc., play significant roles. First of all, the introduction of anti-biofouling polymers such as PEG can reduce the formation of protein corona and therefore preserve the mobility in the blood flow barrier. Meanwhile, the strategy of cell membrane camouflaging can also avoid protein absorption and immune clearance. By utilizing the chemotaxis of neutrophils, biological barrier penetration and specific-site targeting of MNMs have been achieved as well. Importantly, the external physical fields such as magnetic field, ultrasound and light, provide powerful driving forces for the physical field-actuated MNMs to penetrate obstacles. With tunable parameters, these physical fields offer enough driving forces to cross the barriers, for example, cell membrane, vitreous barrier, etc., and even ensure upstream movement in blood flow.

4.1.1. *Hemorheological barrier*

The blood vascular system is a natural network in the body, which promises MNMs arriving at diverse organs and hard-to-reach tissues[40]. Even if the blood vascular system provides the transport route, the hemorheological barrier is still a formidable barrier, except for the opsonization and immune clearance. The harsh physical conditions from hemorheology, such as high flow velocity, variational shear rate and crowded heterogeneous fluid, generally lead to orientation and motion loss of MNMs. The blood flow velocity in arteries ranges from 100 to 600 mm/s. Even in the branches of the inferior vena cava, the blood flow velocity still reaches 500 μm/s, which is much faster than that of MNMs[164]. On the other hand, the diameter of the capillaries is only several micrometers. Therefore, it is difficult to design MNMs that could perform controllable movement in the blood flow.

Recently, inspired by the motion of leukocytes on the surface of a blood vessel, the navigation of MNMs in blood flow has been developed. Alapan et al.[165] reported leukocyte-inspired magnetically actuated micromotors to perform locomotion and cargo delivery under blood flow. The Janus micromotor with a magnetic side rolled on the surface of microchannels which enabled the micromotor to break the symmetry of fluid and perform net displacement. On the other hand, the flow velocity near the no-slip surface was much lower than that at the channel center. Therefore, the micromotor could perform upstream movement under physiological blood flow conditions (shear stress, 2.5 dyn/cm^2). Another side of Janus micromotor with cell-specific antibodies and light-cleavable cargo enabled the recognition of cells and the light-triggered cargo release. This study on upstream motion indicated that MNMs are possible to overcome the hemorheological barrier (Fig. 6A). This strategy can be also utilized *ex vivo*. Wang et al.[166] demonstrated the swarm of nanomotors (Fe_3O_4 nanoparticles) could perform controllable upstream and downstream movement in the porcine coronary artery under blood flow. The nanomotors swarm was achieved under a rotating magnetic field. In the porcine coronary artery, the reduced drag force near the surface is beneficial to the locomotion of nanomotors. More importantly, owing to the localized flow field, which was

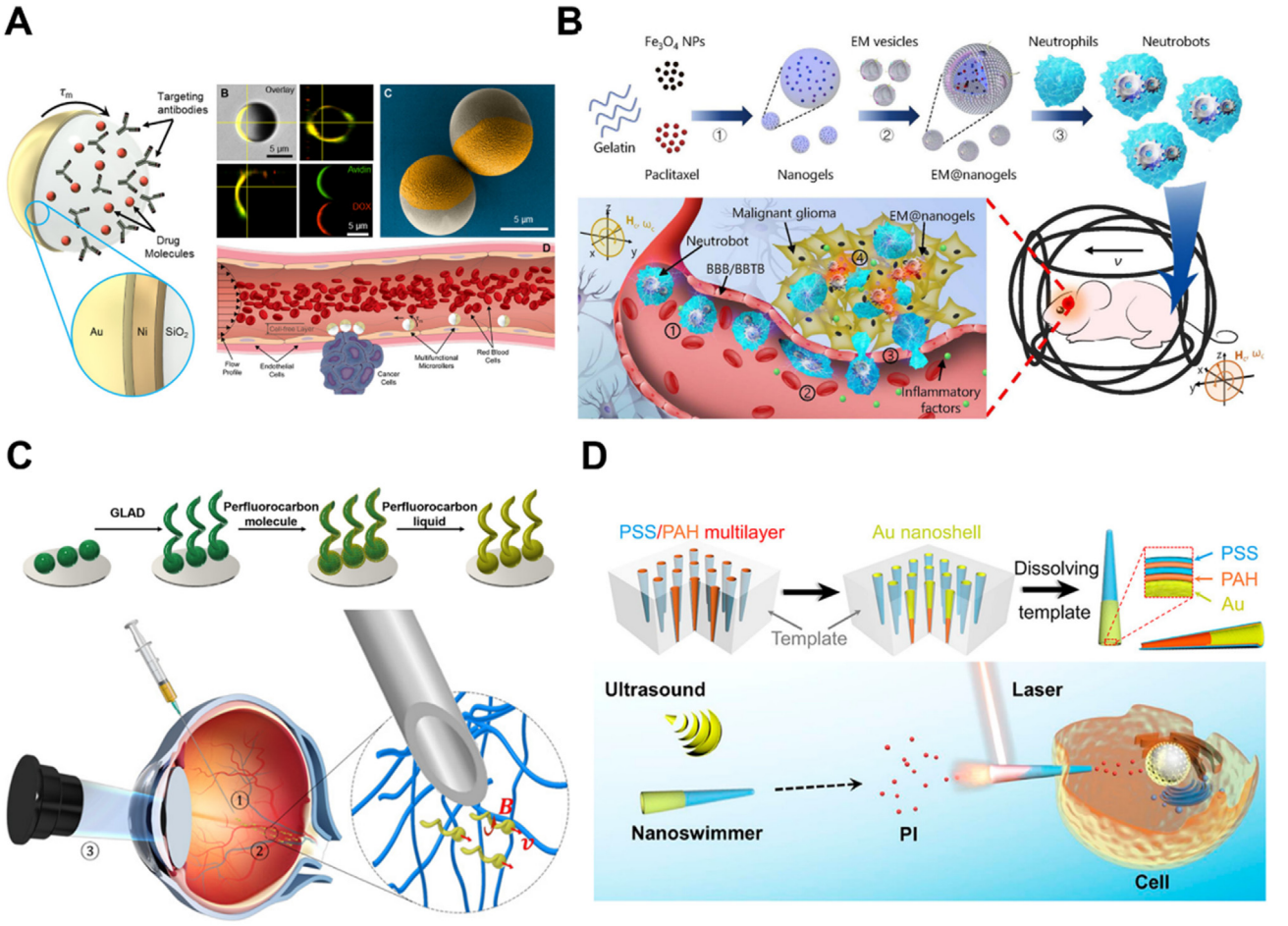

Figure 6 MNMs for overcoming biological barriers. (A) Leukocyte-inspired magnetically actuated micromotors to perform locomotion under blood flow. Reprinted with the permission from Ref. 165. Copyright © 2020 American Association for the Advancement of Science; (B) magnetic field and inflammatory factors-responsive biohybrid neutrobots for crossing the blood−brain barrier. Reprinted with the permission from Ref. 50. Copyright © 2021 American Association for the Advancement of Science; (C) helical magnetically actuated nanomotors for penetrating the vitreous barrier. Reprinted with the permission from Ref. 47. Copyright © 2018 American Association for the Advancement of Science; (D) gold-nanoshell-functionalized conical tubular micromotors for photomechanical poration of cell membrane. Reprinted with the permission from Ref. 173. Copyright © 2019 American Chemical Society.

generated from the swarm, the blood cells near the swarm were disrupted. Therefore, the ultrasound Doppler imaging system could identify the motion of nanomotors in the porcine coronary artery *ex vivo*.

4.1.2. Blood−brain barrier (BBB)

The BBB consists of endothelial cells on the surface of the capillary, astrocyte end-feet of the capillary, and pericytes on the capillary basement membrane, separating the brain from the blood circulation system and protecting the brain from exogenous compounds[167,168]. And thus, MNMs are hard to break through the BBB and reach the brain disease site, such as glioblastoma, resulting in low efficiency of cargo delivery.

Joseph et al.[169] reported enzyme-powered polymeric nanomotors for overcoming the BBB through a chemotaxis strategy. The polymer-based nanomotors were loaded with glucose oxidase and catalase, which could propel the nanomotor by decomposing glucose into D-glucono-δ-lactone and H_2O. Owing to the ability of chemotaxis, the nanomotors moved along the glucose concentration gradient, especially the glucose gradient from the center to the vessel wall. Therefore, the nanomotors could perform chemotactic motion at the blood vessel of brain and cross the BBB due to the glucose gradient at the brain region. A biohybrid micromotor was further demonstrated for the treatment of brain disease by Zhang et al.[50]. The micromotor was fabricated through phagocytosis of natural neutrophils with *E. coli* membrane-enveloped, paclitaxel-loaded magnetic nanogels. Then, the dual-responsive micromotors not only exhibited controllable swarm motion by rotating magnetic field, which accelerated the accumulation at the disease region, but also performed chemotactic behavior to penetrate the BBB. Therefore, the loaded paclitaxel was released at the glioblastoma region, thus improving the efficiency of cargo delivery. These results demonstrate the potential promises of precise therapy for brain disease by MNMs and the breakthrough in overcoming the BBB (Fig. 6B).

4.1.3. Vitreous barrier

The vitreous barrier also limits the delivery route of MNMs, thus reducing the therapeutic effect of eye diseases, such as glaucoma

and diabetic retinopathy. Before reaching the diseased region of the retina, MNMs should penetrate the vitreous body located at the position between the retina and lens. However, a vitreous body that consists of a gelatinous substance with water in a matrix of hyaluronic acid and collagen bundles network limits the locomotion of MNMs. Therefore, the vitreous body is an obvious barrier for MNMs. To address this issue, Wu et al.[47] demonstrated that the helical magnetically actuated nanomotors could penetrate the vitreous barrier and reach the retina. The helical nanomotors with a diameter of 500 nm and length of 2 μm were functionalized with a perfluorocarbon surface. The diameter of nanomotors was comparable to the mesh of the vitreous barrier, and the perfluorocarbon surface minimized the interaction between nanomotors and biopolymers (including collagen bundles) from the vitreous body (Fig. 6C). Through the above design, the nanomotors could perform controllable propulsion in the eyeball and reach the retina within 30 min, which was ~10 times faster than the passive diffusion cargos with comparable size. And the target region on the retina was ~36 mm^2 in area, showing more precision than the passive counterparts.

4.1.4. *Cell membrane barrier*

The cell membrane is the boundary of a living cell, preventing the free entry of extracellular matter. To deliver therapeutic drugs which function on the cytosol or nuclei, MNMs should first break through the cell membrane[170]. Nevertheless, it is difficult for MNMs to penetrate the cell membrane actively due to insufficiency in driving force. To the best of our knowledge, the reported minimum critical stress (σ) for opening cell membrane is around 0.6×10^4 N/m^2, which is more than two orders of magnitude above the applied force from general MNMs[171].

The studies on actively opening cell membranes were carried out by Xuan et al.[172]. They developed NIR light-actuated Janus mesoporous silica nanomotors for thermomechanically percolating the cell membrane. The Janus nanomotors performed self-propulsion in media *via* photothermal effect-induced self-thermophoresis. The diameter of the spherical nanomotor was 70 nm and the applied pressure on the cell membrane was around 1.7 N/m^2. Although the produced pressure was lower than the minimum critical stress, the nanomotors could locally heat the contact site on the cell membrane and increase the fluidity. Therefore, NIR-actuated nanomotors could percolate into the cell. Considering the insufficiency of driving forces, another strategy utilizing hybrid powers was also carried out to overcome the cell membrane barrier. The gold-nanoshell-functionalized conical tubular micromotors were prepared by bottom-up controllable assembly, which performed acoustically actuated locomotion[173]. By regulating ultrasonic frequency, the micromotor could target the cell actively with small opening leading orientation (Fig. 6D). The micromotor could only generate insufficient pressure on the cell membrane with single acoustic propulsion. With the assistance of NIR light on the big opening, the instantaneous photothermal force along the long axis was sufficient (10^4–10^5 N/m^2) to open the cell membrane, and the micromotor could insert into the cell within 0.1 s. However, it should be noted that although the moving ability of MNMs can improve cellular uptake towards tumor cells, whether this enhancement is good for normal cells remains unknown. Nevertheless, these works demonstrated that MNMs are capable of actively targeting the tumor cell and penetrating the cell membrane, showing potential applications in the efficient transportation of various drugs into cells.

4.2. *Biosensing*

Traditional sensing techniques often rely on passive diffusion to capture the targeted analytes. Different from passive ones, MNMs have shown promising prospects in biosensing due to their unique active motion properties and easy functionalization. The movement of MNMs with various receptors can realize “on the fly” capturing analytical targets. Therefore, a variety of advanced biosensing strategies based on MNMs have been developed for different analytes such as small molecules, proteins, nucleic acid and bacterial endotoxins.

Protein detection is of great significance in various fields from biology to medicine. Recently, Ma and coworkers[174] fabricated a nanomotor-assisted immunoassay system for the sensing of immunoglobulin (IgG). Coupling primary antibodies IgG to Fe_3O_4@SiO_2/Pt nanomotors yielded nanomotor labels. Meanwhile, the secondary antibodies were conjugated to Au@Ag nanocubes to obtain Au@Ag NCs-Ab_2 labels. The nanomotor labels could propel in the presence of H_2O_2 and efficiently capture IgG and Au@Ag NCs-Ab_2. The autonomous motion enhanced the immune recognition and resulted in the formation of immune complex which could be measured by differential pulse voltammetry with improved sensitivity (Fig. 7A). Moreover, strategies that combine fluorescence changes with motors are also utilized. Beltran-Gastelum et al.[175] modified the ultrasound-propelled nanomotors with fluorescein-labeled DNA aptamer for the sensing of A1B1 oncoprotein in MCF-7 breast cancer cells. Due to fluorescence resonance energy transfer (FRET), the fluorescence was quenched by graphene oxide. Under the ultrasound activation, the nanomotors were able to move and rapid crosslink with the target protein, resulting in faster fluorescence recovery (Fig. 7B). Furthermore, Mayorga-Martinez’s group[176] fabricated an IrO_2/Pt bilayer microtube through template-assisted electrodeposition. The IrO_2/Pt bilayer microtube acted as both a micromotor and an electrocatalytic tag. Self-propelled tags could capture the target protein and improve the electrochemical detection of protein (Fig. 7C). In addition, de Avila and coworkers[177] reported a dynamic micromotor-based immunoassay for naked-eye detection of cortisol rapidly, which greatly improved the sensitivity and the detection rate. To automate the process of enzyme-linked immunosorbent assay (ELISA), Wang et al.[178] constructed a maneuverable immunoassay probe based on magnetic nanorobots. In this work, they decorated capture antibodies on the surface of rod-like magnetically-driven nanorobots to achieve magnetically maneuverable immunoassay probes (MNR-Ab1s). Meanwhile, a detection unit consisting of different function wells was fabricated by 3D printing. Under a magnetic field, the probe could rotate actively and move between different function wells, which enhanced the binding efficacy and reduced the assay time (Fig. 7D). The simulation of Helmholtz coils produced magnetic field distribution, offering the possibility of this approach to fabricate high throughput nanorobots based ELISA instrument. In another example, changes in micromotors’ movement behavior were transformed into changes in color, thus the production of a colorimetric sensor. Russell et al.[179] used iron oxide to capture the target molecule and remove the non-specific interactions rapidly. The interaction between the target molecule and iron oxide triggered a change in the particles’ motion. Due to the color of iron oxide, this motion behavior was transformed into an observable color change, which could be quantified with a smartphone.

DNA, as genetic information, is a biological macromolecule essential for the development and proper function of organisms.

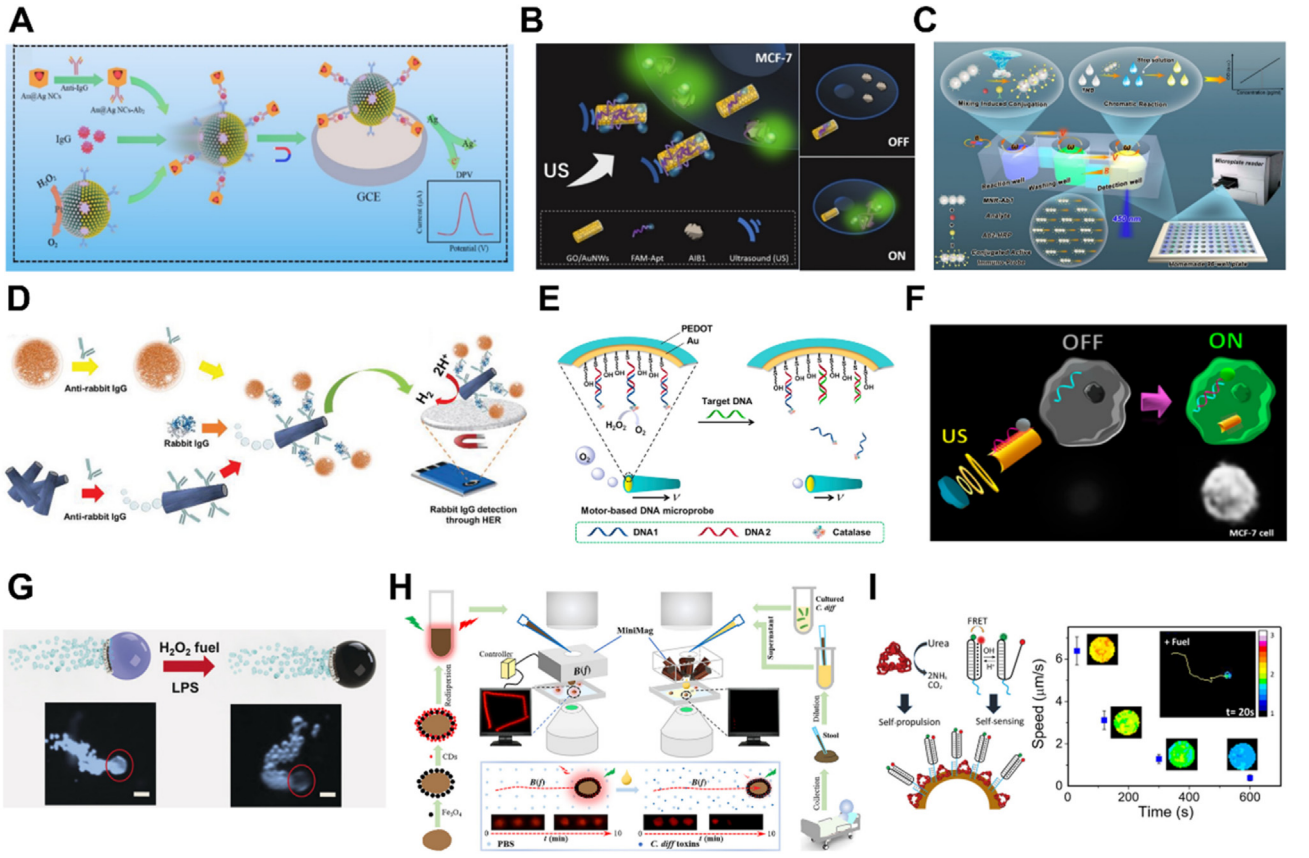

Figure 7 Biosensing strategies based on MNMs. (A) The detection of IgG by Fe_3O_4@SiO_2/Pt nanomotor-assisted immunoassay system. Reprinted with the permission from Ref. 174. Copyright © 2022 Springer−Verlag GmbH Austria; (B) schematic illustration of AIB1 protein detection in breast cancer cells based on the fluorescence change of nanomotors. Reprinted with the permission from Ref. 175. Copyright © 2019 Wiley−VCH; (C) self-propelled IrO_2/Pt bilayer micromotors as tags for protein detection. Reprinted with the permission from Ref. 176. Copyright © 2019 Wiley−VCH; (D) Magnetic nanorobots as maneuverable immunoassay probes for improving the detection efficiency of ELISA. Reprinted with the permission from Ref. 178. Copyright © 2022 American Chemical Society; (E) the changed motion signal of catalase powered micromotor for the detection of the target DNA. Reprinted with the permission from Ref. 180. Copyright © 2016 Elsevier; (F) miRNAs sensing in real time based on the ultrasound propelled nanomotors. Reprinted with the permission from Ref. 183. Copyright © 2015 American Chemical Society; (G) the sensing of bacterial endotoxin using magnetocatalytic graphene quantum dots Janus micromotors. Reprinted with the permission from Ref. 184. Copyright © 2017 Wiley−VCH; (H) spored-derived fluorescent magnetic microrobots for real-time sensing of bacterial toxins. Reprinted with the permission from Ref. 185. Copyright © 2019 American Association for the Advancement of Science; (I) the urease-powered micromotors modified with DNA nanoswitch for sensing the pH change and micromotors intrinsic activity. Reprinted with the permission from Ref. 186. Copyright © 2019 American Chemical Society.

The detection of specific DNA fragments has provided useful information for many diseases. At present, several works have reported the sensing of DNA fragments based on MNMs. Xie et al.[180] assembled a catalase layer on the inner surface of PEDOT/Au microtube through DNA conjugate to construct a catalase catalytic micromotor. When the target DNA was added, the catalase-linked DNA was then replaced, resulting in a decrease of the enzyme's number on the microtubule surface and thus micromotors' speed (Fig. 7E). Therefore, the amount of the target DNA in the solution could be quantified by the moving speed of the micromotor. To improve the sensitivity, catalase was assembled on the surface of PEDOT-PSS/Au microtube[181] and the shell[182] through DNA cyclic alternate hybridization. In addition to DNA, microRNA (miRNA) is a class of endogenous small RNA with approximately 20−24 nucleotides in length, which plays a variety of important regulatory roles in cells. Esteban-Fernandez de Avila et al.[183] for the first time real-time sensed a target miRNA in a single cell by combining the nanomotors and fluorescent change. Dye-labeled ssDNA was immobilized on the surface of graphene oxide (GO); however, the fluorescence was quenched by GO due to the FRET effect. Under the ultrasound, the nanomotors rapidly moved to the cell, and the dye-labeled single-strand DNA was hybridized with the target miRNA-21, resulting in fluorescence recovery (Fig. 7F). Therefore, measuring the fluorescence signal of the ultrasound-propelled nanomotors could monitor the miRNA-21 expression in individual cancer cells.

Bacterial endotoxin is a unique structure on each layer of the gram-negative bacterium cell membrane. Endotoxin is not only the main pathogenic factor of gram-negative bacteria infection but also closely related to many other human diseases. Jurado-Sanchez et al.[184] fabricated a magneto-catalytic Janus micromotor for detecting bacterial endotoxin. They loaded magnetic Fe_3O_4 nanoparticles and Pt nanoparticles on one side of Janus micromotors, followed by encapsulation with graphene quantum

dots (GQDs). The Janus micromotors could be propelled in the presence of H_2O_2 and magnetic actuation. When the micromotors captured the target endotoxin, the fluorescence of GQDs on the micromotors was quenched (Fig. 7G). Furthermore, Zhang et al.[185] reported fluorescent magnetic microrobots made from spores for real-time sensing of bacterial toxins. The micromotors were constructed by the incorporation of Fe_3O_4 nanoparticles and carbon dots on the surface of natural spores. The presence of *Clostridium difficile* (*C. diff*) toxins could be detected by tracking the fluorescence change in real-time (Fig. 7H). To sense the pH value of micromotors' surrounding microenvironment, Patino and coworkers[186] immobilized FRET-labeled triplex DNA nanoswitch that was responsive to pH on the surface of urease-powered micromotors. During the micromotors' self-propulsion, urease catalyzed urea decomposition and caused a rapid change of surrounding pH, which could be detected by observing FRET efficiency through confocal laser scanning microscopy (Fig. 7I).

4.3. Diagnosis

Owing to the small size, active propulsion and motion-based vortex effects, MNMs have been employed for disease diagnosis including biopsy, health monitoring and imaging. They can not only allow for monitoring biological targets at a low concentration with the decrease of required sample volumes and assay time but also enable enhanced signals for target detecting or imaging. Moreover, with subject-capturing ability, MNMs can be fantastic alternatives to detect and retrieve biological samples for pathological analysis, especially for diseased targets in narrow capillaries or lesions deep inside the body.

4.3.1. Biopsy

Conventional biopsy is the gold standard diagnosis to confirm or rule out disease (especially cancer). However, it involves invasive methods that usually cause traumas and pain, which are hardly acceptable to patients. MNMs, as miniaturized motile devices, offer great potential to achieve non-invasive biopsy for diagnosis. In 2009, Leong et al.[187] developed a microrobot that was able to actuate under biologically relevant conditions. It has been proposed for removing cells at a glass capillary (*in vitro* biopsy). Subsequently, they further demonstrated enzymatically triggered robots for external biopsy in liver tissue from a model organ system[188]. In this study, the biopsy action was achieved by the enzymatic degradation-triggered closing and the orthogonal enzyme-actuated reopening of the robot, which allowed for RNA retrieval from cells after capture (Fig. 8A). Even so, the above-mentioned studies did not prove their usage in real organs, especially under *in vivo* conditions. To this end, they fabricated a microrobotic system featured a smaller size for *in vivo* biopsy of a porcine colon, and RNA and DNA could be extracted from the retrieved high-quality tissue samples for cytologic and genetic diagnostics analysis to diagnose cancer, inflammation, and other conditions[189].

4.3.2. Health monitoring

Apart from biopsy, MNMs modified with specific recognition elements can be exploited to detect and identify cancer cells. Distinguishing cancer cells from normal ones is of great significance for clinical diagnosis. Wang et al.[131] prepared a light-powered match-like AgNW@SiO_2 nanomotor as an active SERS probe. These nanomotors could be aggregated quickly owing to the positive phototaxis, which further enhances the SERS signal. Using these nanomotors, the biological Raman signals of the cancer cells could be captured clearly (Fig. 8B). Then the same group[190] also reported a rod-like magnetic nanomotor as a maneuverable SERS probe. The synthesized magnetic nanomotors could be navigated to the target sites and own the ability of self-cleaning. Due to the effective mixing, the nanomotors could capture more intracellular Raman signals. Zhao et al.[191] decorated catalase on the surface of Janus rods to construct micromotors for capturing circulating tumor cells (CTCs). They conjugated thymine and guanine on tetraphenylethene (TPE) and fluorescein isothiocyanate (FITC), which were used for aptamer grafting through base−pair interaction. The binding of CTCs with aptamer triggered the release of TPE and FITC, resulting in the change of fluorescence signals.

Additionally, MNMs are attracting candidates for diagnosing infectious diseases caused by microorganisms as well. Olson et al.[192] developed a catalase-coated silica nanomotor for pinpointing the location of microbial abscesses. The motor was powered by the decomposition of hydrogen peroxide, and the fuel concentration was high in the inflamed microbial abscess. The produced oxygen microbubbles could be visualized by ultrasound imaging, and thus indicated the diseased location. Moreover, the suitable use of the recognition elements toward a certain kind of microorganism enables the selective recognition of the microorganism. Typically, concanavalin A (ConA), a kind of lectin, can specifically target gram-negative bacteria[193]. Campuzano and coworkers[194] fabricated a kind of microtubular motor modified with ConA for specific identification and isolation of gram-negative bacteria. The self-propelled motor powered by the decomposition of H_2O_2 could recognize *E. coli* bacteria in the samples while the *Saccharomyces cerevisiae* cells could not be captured. Recently, MNMs were also used for virus infections monitor. Draz and coworkers[195] fabricated a nanomotor-based bead motion cellphone (NBC) system to detect the Zika virus rapidly. The presence of the virus induced the assembling of Pt nanomotors onto the surface of 3 μm polystyrene (PS) beads. The formed immunocomplex could be propelled in the presence of H_2O_2 and the velocity was measured by a cellphone with an optical attachment and a motion tracking application (Fig. 8C). The movement speed was directly related to the concentration of the virus.

4.3.3. Imaging

MNMs can also be employed in imaging for diagnosis to obtain images with high details. For instance, MNMs have been considered active diagnostic agents for enhanced magnetic resonance imaging of tumor tissues *in vivo*[196]. The developed nanomotors were able to actively target, adhere and perforate tumor cells, and thus improve cellular uptake and MR imaging. In addition, *in vivo* studies revealed high accumulation and deep penetration of the nanomotors in the solid tumor model, notably enhancing the MR imaging contrast in the majority of the tumor tissue (Fig. 8D). Therefore, MNMs would provide a novel strategy for precise cancer diagnosis and MR imaging offers a tracking approach of nanomotors *in vivo*. Besides, MNMs also demonstrate enhanced performance in ultrasonic imaging. Feng et al.[197] succeeded in improving the contrast of ultrasonic imaging using a multi-responsive Mg/Ni micromotor. The component Ni provided magnetic navigation of the motor to the targeted lesion while Mg offered strong propulsion based on the spontaneous Mg-water reaction in the acid-base environment. The generated H_2 microbubbles could be used for ultrasonic imaging. Meanwhile, these

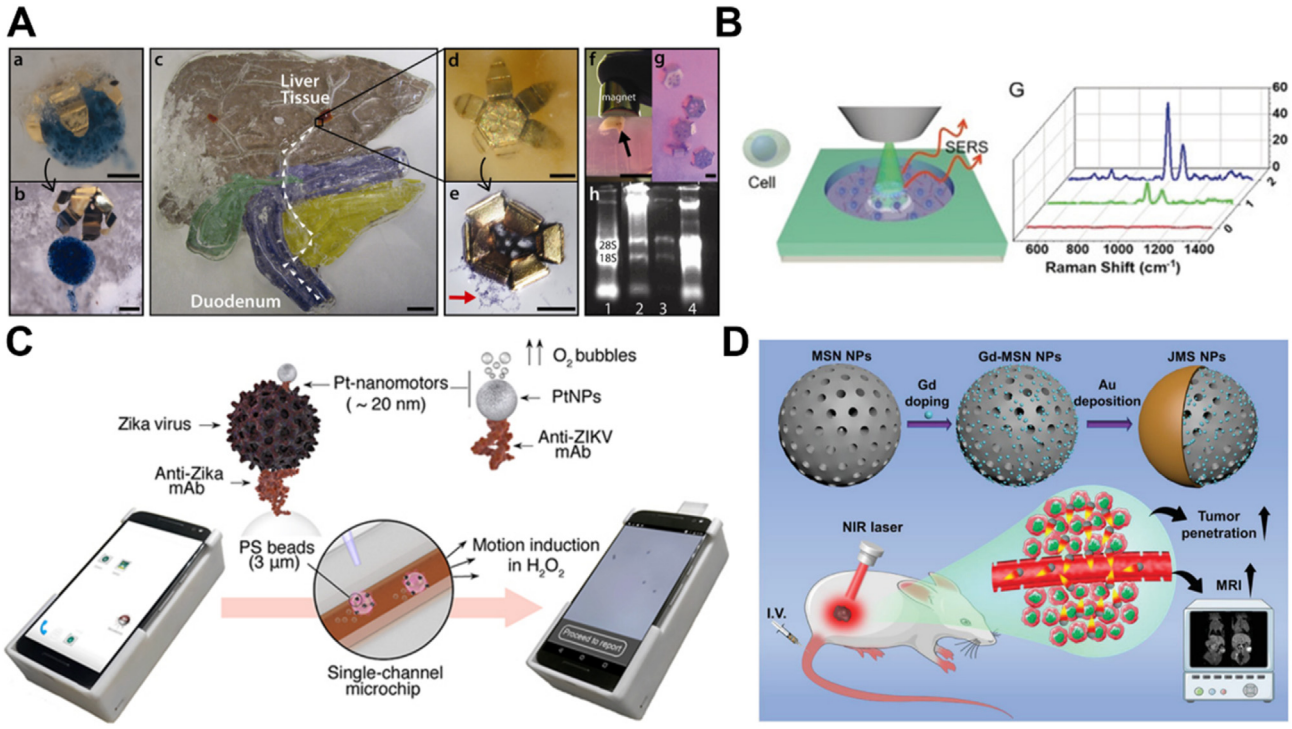

Figure 8 MNMs for diagnosis. (A) MNMs for external biopsy in a liver tissue from a model organ system, and RNA retrieval from captured cells. Reprinted with the permission from Ref. 188. Copyright © 2010 American Chemical Society; (B) capture of biological Raman signals of the cancer cells using photocatalytically powered match-like nanomotors. Reprinted with the permission from Ref. 131. Copyright © 2018 Wiley−VCH; (C) the detection of Zika virus by the change in the velocity of Pt-nanomotors. Reprinted with the permission from Ref. 195. Copyright © 2018 American Chemical Society; (D) MNMs as active diagnostic imaging agents for enhanced magnetic resonance imaging of tumor tissues. Reprinted with the permission from Ref. 196. Copyright © 2021 Wiley−VCH.

micromotors were possible to move towards nodes or antinodes and form aggregates with concentrated bubbles in the presence of an ultrasound field, resulting in enhanced ultrasonic contrast.

4.4. *Minimally invasive microsurgery*

In the 1980s, the concept of minimally invasive surgery with smaller cuts or incisions emerged, which mainly expects a precise, safe and effective surgical procedure[198]. As emerging miniaturized devices, MNMs capable of active motion and superior controllability are suitable for microsurgery, thus offering more precise operations, shorter recovery time and less postoperative pain[199].

Solovev's team[200] developed a rolled-up nanomotor that was able to achieve surgical tasks towards a single cell. The motor consisted of catalytic InGaAs/GaAs/(Cr)Pt components, in which Pt could catalyze the decomposition of H_2O_2 and provide efficient power for movement with speeds as high as 180 μm/s. The rolled-up motor with cylindrical shape moved in a straight line, while the asymmetrically rolled-up shape permitted a powerful corkscrew-like moving pattern, enabling effective drilling into substrates such as a single cell (Fig. 9A). However, as high concentration of H_2O_2 is toxic for body, the same team developed a magnetic microtool for microsurgery[43]. By tuning the frequency of the applied magnetic field, a stabbing/drill-like manner towards a single cell was achieved. Recently, Jin et al.[201] succeeded in manipulating individual or a few cells using a thermo/magnetic-responsive microrobot. They engineered this system with SiO_2 as the differential stress layer, and paraffin for thermally facilitating the release of the stored differential stress. The bending rigidity of the wax layer was sensitive to temperature, and it would decrease as the temperature increased, leading to the grasping action. Meanwhile, a magnetic layer was introduced to allow remote magnetic control. In cell environments, this microrobot could perform a series of precise surgical procedures, including grasping a single cell or a few cells upon temperature increase, and dragging the cells away by magnetic control (Fig. 9B). However, it is worth noting that as this active action can achieve physical manipulation towards a cell, it should be performed very carefully otherwise it may cause harm to normal cells or tissues.

In addition to cell level, MNMs also showed potential *ex vivo* and *in vivo* applications in the field of minimally invasive surgery. For traditional invasive surgery towards a body, procedures are normally hard to operate in deep tissue regions. With miniaturized structures and powerful penetration ability, MNMs offer significant opportunities to achieve non-invasive surgery. Xi et al.[53] built a magnetic micromotor that could drill and perform incision operations toward porcine liver tissue. This micromotor was fabricated with Ti/Cr/Fe components, where Fe provided magnetic functions and Ti/Cr facilitated rolled-up morphology. With an external magnetic field, this tubular microdriller could be manipulated from lying to walking, offering drilling operations for surgery. The controllable drilling manner could last from tens of minutes to a few hours, thus incising holes effectively toward the tissue (Fig. 9C). Apart from the magnetic field, ultrasound is also

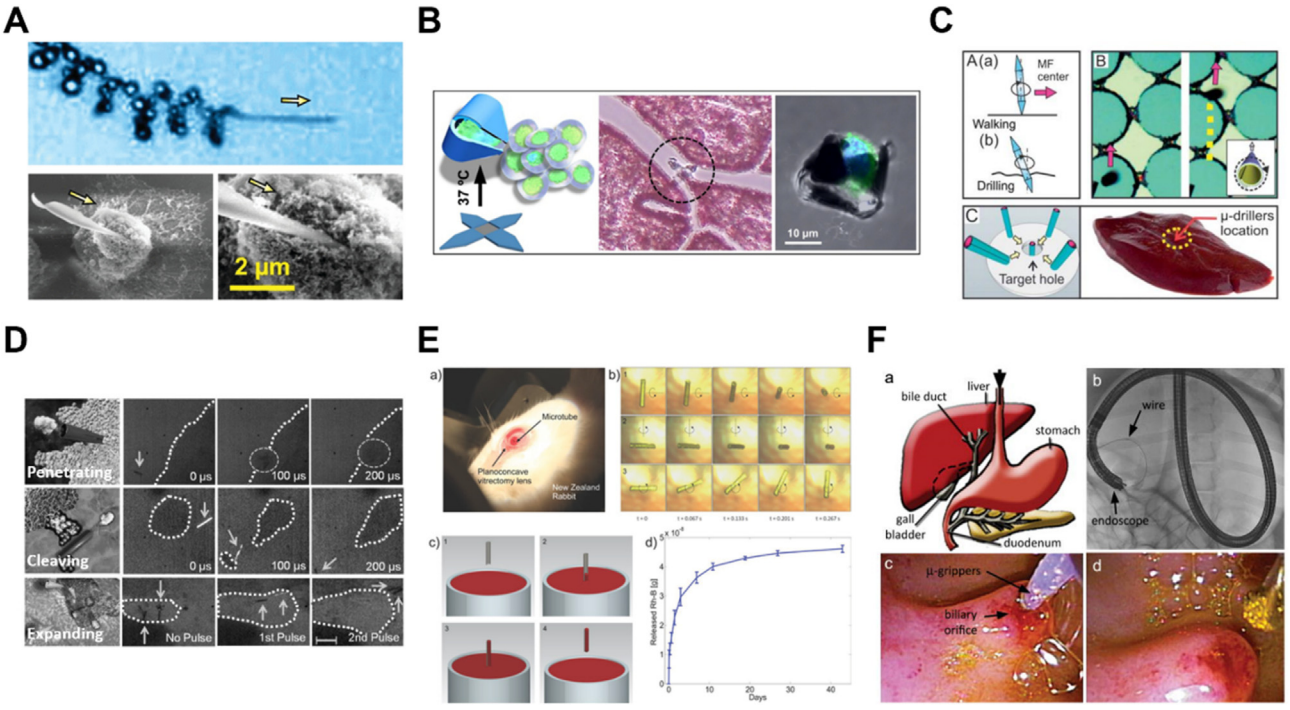

Figure 9 MNMs for minimally invasive microsurgery. (A) A self-propelled nanotool that drilled into a cell. Reprinted with the permission from Ref. 200. Copyright © 2012 American Chemical Society; (B) a thermo/magnetic-responsive micromotor for manipulating a single cell or a few cells. Reprinted with the permission from Ref. 201. Copyright © 2020 American Chemical Society; (C) a magnetic micromotor that drilled and performed incision operations toward a porcine liver tissue. Reprinted with the permission from Ref. 53. Copyright © 2013 Royal Society of Chemistry; (D) a PFC-loaded microbullet propelled by ultrasound for penetrating, cleaving and expanding a tissue. Reprinted with the permission from Ref. 52. Copyright © 2012 Wiley−VCH; (E) An implantable micromotor enabling rotational movements and drug delivery in a living rabbit eye. Reprinted with the permission from Ref. 202. Copyright © 2014 Wiley−VCH; (F) A star-shaped tetherless microgripper. Reprinted with the permission from Ref. 203. Copyright © 2013 Wiley−VCH.

considered a strong energy source for driving a motor. Kagan et al.[52] reported a powerful perfluorocarbon (PFC)-loaded microbullet propelled by ultrasound for non-invasive precision nanosurgery, including penetrating, cleaving and expanding a tissue. The micromotor was first prepared by rolled-up nanofabrication techniques with an embedded Ni magnetic layer and an inner Au layer. The Ni permitted a convenient purification process as well as wirelessly magnetic-guided precision steering, while the Au layer allowed cysteamine conjugation for the attachment of PFC emulsion. Under the ultrasound, PFC droplets vaporized and ejected the motor like a bullet, with a significant high speed of over 6 m/s (160,000 body lengths per second). This remarkable speed and resulting force enabled strong tissue piercing, deep penetration and cleaving capabilities (Fig. 9D). In the field of eye diseases, Chatzipirpiridis and coworkers[202] reported a kind of implantable micromotor for wireless ophthalmologic surgery. The motor was constructed through an electroforming approach with CoNi ingredients for magnetic field-powered propulsion. Through a needle, this motor could be injected into the central vitreous humor of a living rabbit eye. When subjected to magnetic torques and forces, the motor was able to perform intravitreal operations including rotation and translation. These controllable operations along with the convenient approach, indicated a promising minimally invasive surgery strategy for ophthalmologic diseases (Fig. 9E).

In addition, MNMs also demonstrated great potential for surgery on gastroenterological diseases. A set of tetherless microgrippers have been developed for gastroenterological surgery in live animals[189,203]. Tetherless microgrippers are a kind of important microrobots for minimally invasive surgery. As conventional microgrippers are tethered and have restricted miniaturization and maneuverability, untethered microgrippers are usually navigated by wireless external fields and actuated by body stimuli (*e.g.*, temperature), offering great chances to perform precise microsurgery in a narrow tissue space[204]. For instance, Gultepe et al.[203] fabricated a star-shaped tetherless microgripper that could reach a narrow bile duct and perform precise actions. Engineered with chromium and gold bilayer hinges, this microgripper was powered by the residual stress in the hinges which was constrained *via* a thermal polymeric trigger. Upon exposure to body temperature, the polymer became soft and the hinges launched spontaneous curving, leading to gripping action. After being delivered by a catheter into the biliary orifice, this device was able to perform gripping and excising manners in a hard-to-reach place (Fig. 9F). Such tether-free microsurgical tools enabled precise surgical procedures with minimal trauma.

4.5. *Targeted cargo delivery*

In view of the defects of traditional drug delivery systems, such as short drug retention time and poor tissue permeability, active MNMs loaded with drugs can improve cellular uptake with the help of autonomous movement and penetrate physiological barriers, thus enabling enhanced therapeutic effect[205,206]. It should be

noted that the drugs here are not limited to traditional small molecule drugs, but also include photothermal therapeutic agents, functional proteins, cells (sperm), etc[207−210].

Normally the pathological microenvironment and the structural characteristics of diseased organs or tissues vary, which determine the selection of administration approach for a certain disease. Using the gastric acid provided by the gastrointestinal environment, acid-powered MNMs with high loading capacity and non-toxic self-destruction property are becoming the focus of current research. The drug-loaded micromotors developed by researchers[49,211,212] could be effectively embedded into the mucosal lining of gastrointestinal tissue due to autonomous movement, which further prolonged the drug residence time and thus enhanced the therapeutic effect. Later, Li et al.[213] designed a magnesium-based micromotor capable of propelling in gastric juice by rapid consumption of local protons. By automatic and temporary neutralization of gastric acid, this system became an attractive alternative to proton pump inhibitors. In addition, the surface of this micromotor was coated with cargoes containing a pH-responsive polymer layer, enabling the site-specific drug release without causing obvious acute toxicity or affecting gastric function. On this basis, the same team[212] further developed a drug-loaded magnesium micromotor that could neutralize gastric acid and treat gastrointestinal *Helicobacter pylori* infection in a mouse model without using proton pump inhibitors (Fig. 10A). In this motor, the commercial antibiotic drug clarithromycin (CLR) was loaded with high efficiency to kill *H. pylori*. Besides, the active propulsion of the micromotor could enhance the retention of the drug in the stomach, resulting in improved *in vivo* therapeutic effects. To achieve acidic gastric resistance, the same group[211] developed another magnesium-based motor modified by enteric coating for the intestinal application. The enteric polymer coating enabled the survival of motors in an acidic gastric juice environment (pH 1−3) and the motion activation in intestinal fluid (pH 6−7). Thus, penetration and retention in the intestine could be realized, providing the possibility of personalized treatment. Besides active drug delivery, Wei et al.[214] further modified magnesium micromotors with bionic cell membranes for active delivery of an oral antiviral vaccine. When administered orally to experimental mice, the active propulsion of the micromotor could greatly improve the retention and absorption of antigen substances in the small intestine (Fig. 10B), thus promoting enhanced mucosal immunity.

For cardiovascular diseases, venous thrombosis and atherosclerosis (AS) seriously threaten the health of patients. The clinical drugs for the treatment of these diseases have some disadvantages such as short half-life, low bioavailability and poor penetration at the thrombus sites. To achieve short-term thrombolysis and long-term anticoagulation, Wan et al.[82] reported a platelet membrane-modified nanomotor with a hierarchical pore structure, which was loaded with the clinical thrombolytic drug urokinase and anticoagulant drug heparin (Fig. 10C). Based on the *in vitro* test, the penetration depth of these nanomotors in thrombus was increased almost 3 times when compared with that of passive counterparts. And the retention rate of the active nanomotor was also improved. Moreover, unlike the frequent administration used in the clinic, this motor achieved sequential drug release, including the rapid release of urokinase and slow release of heparin. This allows short-time thrombolysis and long-term anticoagulation. Besides, they also constructed a NO-driven nanomotor to enhance endothelial function, reduce AS plaque lipid deposition and foam cell formation[215]. The immobilized gold nanoparticles on the surface of this nanomotor with photothermal conversion further endowed NIR light-driven motion capability and ablation effect of plaque inflammatory macrophages. The designed nanomotors with dual-driving modes could promote the penetration and retention of therapeutic agents, as well as multi-channel regulation of the atherosclerotic pathological microenvironment.

There are still many difficulties in the treatment of tumors by traditional nanocarriers mainly due to the existing physical obstacles encountered in solid tumors, such as abnormal blood supply, elevated interstitial pressure and large transmission distance in tumor stroma[216,217]. Ye and coworkers[218] constructed a DNase-functionalized Janus nanomotor system powered by extremely low levels of DNA (nmol/L to μmol/L). The nanomotors exhibited chemotaxis towards DNA gradient generated by apoptotic tumor cells, which promises to shed new light on tumor diagnosis and therapy. Moreover, Wan et al.[44] reported a nanomotor-based strategy to improve the chemotherapeutic efficacy of the solid tumor. During the fabrication process, the clinical drug adriamycin was loaded in the nanomotor, along with folic acid for tumor targeting and L-arginine for the moving fuel. With the help of the autonomous movement driven by NO (produced by the decomposition of L-arginine), the motor realized deep penetration of drugs and effective reversal of multidrug resistance in tumors (Fig. 10D). Subsequently, the same group[219] extended the application to cancer immunotherapy. They developed a similar NO-driven nanomotor for the normalization of tumor blood vessels and the degradation of endogenous extracellular matrix, thus significantly promoting the tumor infiltration ability of immune cells *in vivo*. In addition, Li and coworkers[220] developed a nanomotor based on DNA origami technology. The motors could accurately locate tumor cells with thrombin, block the blood supply to inhibit tumor growth and metastasis without causing an obvious immune response, which is potential for many types of tumors. Besides, MNMs also demonstrated great potential for brain tumors. Deng et al.[221] designed and applied natural-killer-cell-inspired nanorobots with aggregation-induced emission characteristics for diagnosis and treatment of glioma. The nanomotors could penetrate the BBB efficiently, diagnose glioma with high contrast, and achieve effective photothermal therapy for glioma.

5. Future perspective and challenges

Medical MNMs may access hard-to-reach parts of the body and promise broad potential applications in the field of biomedicine owing to their micro-/nano size and active motion abilities. To meet the practical medical application, in this review, we summarized and discussed many challenges and relevant breakthroughs in medical MNMs not only in the design and fabrication but also in the various bio-applications. However, it is still difficult to overcome the biological barriers, and the existing technologies of navigation and real-time tracking could not meet the practical requirements *in vivo*. To address the issues, further developments of MNMs should be executed.

Biocompatibility and biodegradability are the basic principles of medical MNMs. Biocompatible and biodegradable synthetic or

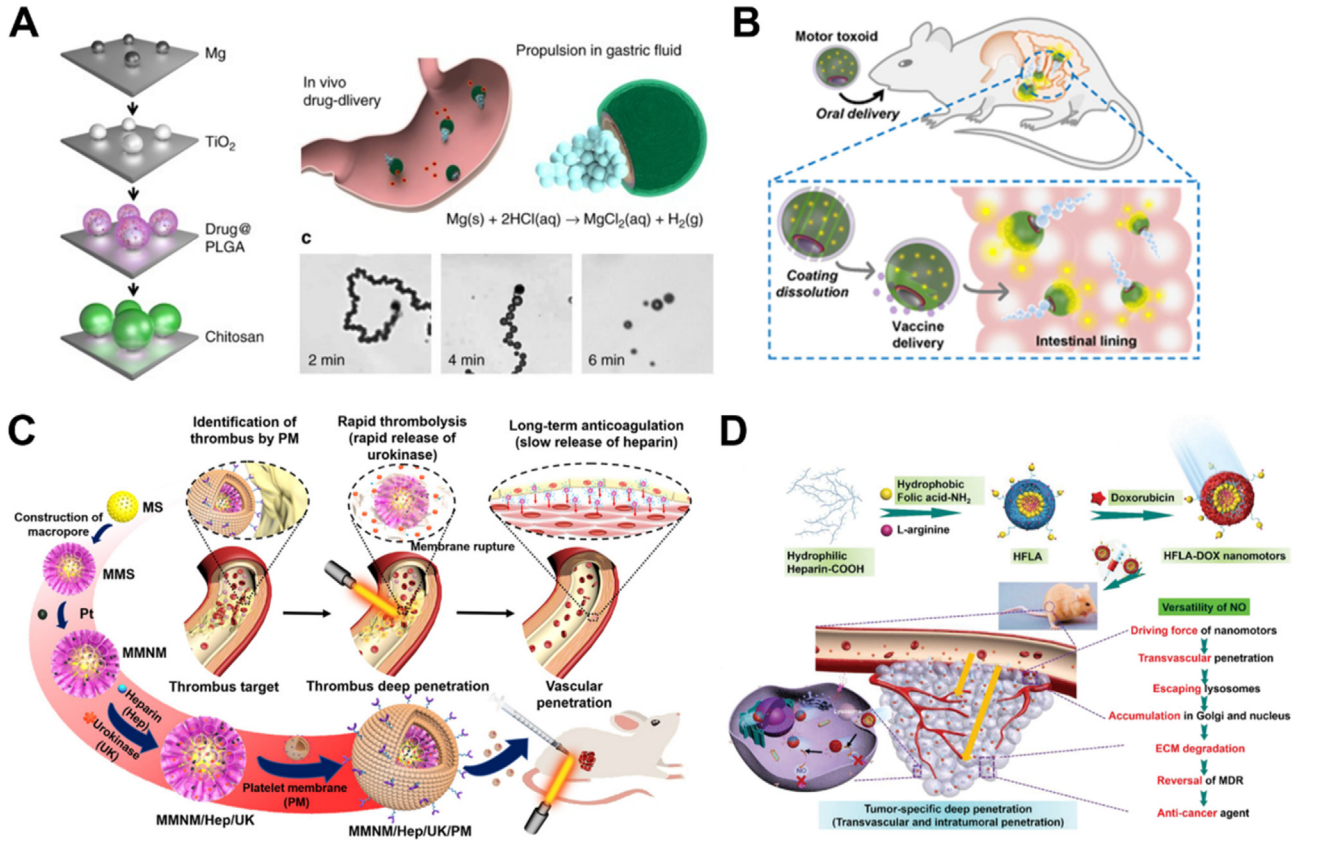

Figure 10 MNMs for targeted cargo delivery. (A) Drug-loaded Mg-based micromotors for treatment of stomach infection. Reprinted with the permission from Ref. 212. Copyright © 2017 Nature Publishing Group; (B) a micromotor enabling active delivery of antigens for oral vaccination. Reprinted with the permission from Ref. 214. Copyright © 2019 American Chemical Society; (C) a nanomotor loaded with thrombolytic and anticoagulant drugs to achieve short-term thrombolysis and long-term anticoagulation. Reprinted with the permission from Ref. 82. Copyright © 2020 American Association for the Advancement of Science; (D) adriamycin/folic acid/L-arginine nanomotors for enhanced tumor chemotherapy. Reprinted with the permission from Ref. 44. Copyright © 2020 Wiley−VCH.

natural materials should be used as building blocks for the design of MNMs. Fortunately, scientists have been aware of this and initiated some works, such as the incorporation of biocompatible and biodegradable polymers (PEG, PLGA, PCL) while fabricating medical MNMs. However, more basic needs to be clarified, including the biodegradable manners, the pharmacokinetics, the relations between the *in vivo* behavior and the property of the used materials, etc. Moreover, chemical propulsion should choose non-toxic fuel especially endogenous substrate, and fuel-free propulsion should also avoid the potential damage to normal tissues. For example, endogenous substrates including H_2O, gastric acid, urea, glucose, etc., need more attention, and the effective propulsion of MNMs at the *in vivo* substrate level is supposed to be guaranteed. Besides, when using fuel-free strategies, the *in vitro* and *in vivo* safety intensity or parameters of the applied fields have to be optimized in detail. Towards the biological environment, the conditions of navigation are harsh for MNMs. Many navigation strategies which work well *in vitro* are unsuitable in bodies due to the various biological barriers. Therefore, a disease-specific strategy that is possible to overcome the surrounding biological barrier and microenvironment is necessary for MNMs. For example, MNMs aiming for glioma therapy should overcome the BBB, and MNMs which are designed for thrombolysis should avoid the immune clearance and overcome the hemorheological barrier. Overcoming these barriers can increase the accumulation of MNMs at the target sites, leading to enhanced therapeutic efficacy. On the other hand, the research on navigation and overcoming biological barriers cannot be separated from real-time tracking. The present technologies, such as fluorescence imaging, ultrasonic imaging and magnetic resonance imaging, still have quite some limitations in tracking speed, penetration depth, or other aspects. Therefore, in the complex biological environment, medical MNMs still face multiple challenges. With more systematic and accurate studies, it is believed that the medical MNMs will meet the practical medical application and carry out tasks of diagnosis and therapy.

Acknowledgments

This study was supported by the National Natural Science Foundation of China (Grant No. 22175083, 51973241, 82001845, 52072095, 92163109 and 22193033).

Author contributions

Huaan Li, Fei Peng, Xiaohui Yan, Chun Mao, Xing Ma, Daniela A. Wilson, Qiang He and Yingfeng Tu: manuscript drafting and revision.

Conflicts of interest

The authors declare no conflicts of interest.

References

1. Vale RD, Milligan RA. The way things move: looking under the hood of molecular motor proteins. *Science* 2000;**288**:88−95.
2. Kim K, Guo JH, Liang ZX, Fan DL. Artificial micro/nanomachines for bioapplications: biochemical delivery and diagnostic sensing. *Adv Funct Mater* 2018;**28**:1705867.
3. Peng F, Tu YF, Wilson DA. Micro/nanomotors towards *in vivo* application: cell, tissue and biofluid. *Chem Soc Rev* 2017;**46**:5289−310.
4. Ma X, Jannasch A, Albrecht UR, Hahn K, Miguel-Lopez A, Schaffer E, et al. Enzyme-powered hollow mesoporous Janus nanomotors. *Nano Lett* 2015;**15**:7043−50.
5. Magdanz V, Stoychev G, Ionov L, Sanchez S, Schmidt OG. Stimuli-responsive microjets with reconfigurable shape. *Angew Chem Int Ed* 2014;**53**:2673−7.
6. Pantarotto D, Browne WR, Feringa BL. Autonomous propulsion of carbon nanotubes powered by a multienzyme ensemble. *Chem Commun* 2008:1533−5.
7. Ma X, Wang X, Hahn K, Sanchez S. Motion control of urea-powered biocompatible hollow microcapsules. *ACS Nano* 2016;**10**:3597−605.
8. Hortelao AC, Simo C, Guix M, Guallar-Garrido S, Julian E, Vilela D, et al. Swarming behavior and *in vivo* monitoring of enzymatic nanomotors within the bladder. *Sci Robot* 2021;**6**:eabd2823.
9. Gao W, Pei A, Wang J. Water-driven micromotors. *ACS Nano* 2012;**6**:8432−8.
10. Xu C, Wang SH, Wang H, Liu K, Zhang SY, Chen B, et al. Magnesium-based micromotors as hydrogen generators for precise rheumatoid arthritis therapy. *Nano Lett* 2021;**21**:1982−91.
11. Kline TR, Paxton WF, Mallouk TE, Sen A. Catalytic nanomotors: remote-controlled autonomous movement of striped metallic nanorods. *Angew Chem Int Ed Engl* 2005;**44**:744−6.
12. Dreyfus R, Baudry J, Roper ML, Fermigier M, Stone HA, Bibette J. Microscopic artificial swimmers. *Nature* 2005;**437**:862−5.
13. Gao W, Sattayasamitsathit S, Manesh KM, Weihs D, Wang J. Magnetically powered flexible metal nanowire motors. *J Am Chem Soc* 2010;**132**:14403−5.
14. Yan XH, Zhou Q, Yu JF, Xu TT, Deng Y, Tang T, et al. Magnetite nanostructured porous hollow helical microswimmers for targeted delivery. *Adv Funct Mater* 2015;**25**:5333−42.
15. Chang ST, Beaumont E, Petsev DN, Velev OD. Remotely powered distributed microfluidic pumps and mixers based on miniature diodes. *Lab Chip* 2008;**8**:117−24.
16. Calvo-Marzal P, Sattayasamitsathit S, Balasubramanian S, Windmiller JR, Dao C, Wang J. Propulsion of nanowire diodes. *Chem Commun* 2010;**46**:1623−4.
17. Dai BH, Wang JZ, Xiong Z, Zhan XJ, Dai W, Li CC, et al. Programmable artificial phototactic microswimmer. *Nat Nanotechnol* 2016;**11**:1087−92.
18. Xu LL, Mou FZ, Gong HT, Luo M, Guan JG. Light-driven micro/nanomotors: from fundamentals to applications. *Chem Soc Rev* 2017;**46**:6905−26.
19. Xu TL, Soto F, Gao W, Garcia-Gradilla V, Li JX, Zhang XJ, et al. Ultrasound-modulated bubble propulsion of chemically powered microengines. *J Am Chem Soc* 2014;**136**:8552−5.
20. Uygun M, Jurado-Sanchez B, Uygun DA, Singh VV, Zhang LF, Wang J. Ultrasound-propelled nanowire motors enhance asparaginase enzymatic activity against cancer cells. *Nanoscale* 2017;**9**:18423−9.
21. Venugopalan PL, Esteban-Fernandez de Avila B, Pal M, Ghosh A, Wang J. Fantastic voyage of nanomotors into the cell. *ACS Nano* 2020;**14**:9423−39.
22. Ismagilov RF, Schwartz A, Bowden N, Whitesides GM. Autonomous movement and self-assembly. *Angew Chem Int Edit* 2002;**41**:652−4.
23. Paxton WF, Kistler KC, Olmeda CC, Sen A, St Angelo SK, Cao Y, et al. Catalytic nanomotors: autonomous movement of striped nanorods. *J Am Chem Soc* 2004;**126**:13424−31.
24. Gao W, Pei A, Dong RF, Wang J. Catalytic iridium-based Janus micromotors powered by ultralow levels of chemical fuels. *J Am Chem Soc* 2014;**136**:2276−9.
25. Tu YF, Peng F, Sui XF, Men YJ, White PB, van Hest JCM, et al. Self-propelled supramolecular nanomotors with temperature-responsive speed regulation. *Nat Chem* 2017;**9**:480−6.
26. Wang JM, Toebes BJ, Plachokova AS, Liu Q, Deng DM, Jansen JA, et al. Self-propelled PLGA micromotor with chemotactic response to inflammation. *Adv Healthc Mater* 2020;**9**:e1901710.
27. Wu ZG, Li JX, de Avila BEF, Li TL, Gao WW, He Q, et al. Water-powered cell-mimicking Janus micromotor. *Adv Funct Mater* 2015;**25**:7497−501.
28. Gao CY, Lin ZH, Lin XK, He Q. Cell membrane-camouflaged colloid motors for biomedical applications. *Adv Ther* 2018;**1**:1800056.
29. Tang SS, Zhang FY, Gong H, Wei FN, Zhuang J, Karshalev E, et al. Enzyme-powered Janus platelet cell robots for active and targeted drug delivery. *Sci Robot* 2020;**5**:eaba6137.
30. Dong RF, Zhang QL, Gao W, Pei A, Ren BY. Highly efficient light-driven TiO_2-Au Janus micromotors. *ACS Nano* 2016;**10**:839−44.
31. Gao W, Pei A, Feng XM, Hennessy C, Wang J. Organized self-assembly of Janus micromotors with hydrophobic hemispheres. *J Am Chem Soc* 2013;**135**:998−1001.
32. Gao W, Sattayasamitsathit S, Orozco J, Wang J. Highly efficient catalytic microengines: template electrosynthesis of polyaniline/platinum microtubes. *J Am Chem Soc* 2011;**133**:11862−4.
33. Solovev AA, Sanchez S, Pumera M, Mei YF, Schmidt OG. Magnetic control of tubular catalytic microbots for the transport, assembly, and delivery of micro-objects. *Adv Funct Mater* 2010;**20**:2430−5.
34. Wang W, Castro LA, Hoyos M, Mallouk TE. Autonomous motion of metallic microrods propelled by ultrasound. *ACS Nano* 2012;**6**:6122−32.
35. Ghosh A, Fischer P. Controlled propulsion of artificial magnetic nanostructured propellers. *Nano Lett* 2009;**9**:2243−5.
36. Wang Z, Fu DM, Xie DZ, Fu SM, Wu JY, Wang SH, et al. Magnetic helical hydrogel motor for directing T cell chemotaxis. *Adv Funct Mater* 2021;**31**:2101648.
37. You M, Chen CR, Xu LL, Mou FZ, Guan JG. Intelligent micro/nanomotors with taxis. *Acc Chem Res* 2018;**51**:3006−14.
38. Tu YF, Peng F, Wilson DA. Motion manipulation of micro- and nanomotors. *Adv Mater* 2017;**29**:1701970.
39. Li JX, Esteban-Fernandez de Avila B, Gao W, Zhang LF, Wang J. Micro/nanorobots for biomedicine: delivery, surgery, sensing, and detoxification. *Sci Robot* 2017;**2**:eaam6431.
40. Gao CY, Wang Y, Ye ZH, Lin ZH, Ma X, He Q. Biomedical micro-/nanomotors: from overcoming biological barriers to *in vivo* imaging. *Adv Mater* 2021;**33**:e2000512.
41. Cao SP, Shao JX, Wu HL, Song SD, De Martino MT, Pijpers IAB, et al. Photoactivated nanomotors *via* aggregation induced emission for enhanced phototherapy. *Nat Commun* 2021;**12**:2077.
42. Xuan MJ, Shao JX, Lin XK, Dai LR, He Q. Self-propelled Janus mesoporous silica nanomotors with sub-100 nm diameters for drug encapsulation and delivery. *ChemPhysChem* 2014;**15**:2255−60.
43. Srivastava SK, Medina-Sanchez M, Koch B, Schmidt OG. Medibots: dual-action biogenic microdaggers for single-cell surgery and drug release. *Adv Mater* 2016;**28**:832−7.
44. Wan MM, Chen H, Da Wang Z, Liu ZY, Yu YQ, Li L, et al. Nitric oxide-driven nanomotor for deep tissue penetration and multidrug resistance reversal in cancer therapy. *Adv Sci* 2020;**8**:2002525.
45. Jiao XY, Wang ZM, Xiu JD, Dai WH, Zhao L, Xu TL, et al. NIR powered Janus nanocarrier for deep tumor penetration. *Appl Mater Today* 2020;**18**:100504.
46. Peng F, Men YJ, Tu YF, Chen YM, Wilson DA. Nanomotor-based strategy for enhanced penetration across vasculature model. *Adv Funct Mater* 2018;**28**:1706117.

47. Wu ZG, Troll J, Jeong HH, Wei Q, Stang M, Ziemssen F, et al. A swarm of slippery micropropellers penetrates the vitreous body of the eye. *Sci Adv* 2018;**4**:eaat4388.
48. Walker D, Kasdorf BT, Jeong HH, Lieleg O, Fischer P. Enzymatically active biomimetic micropropellers for the penetration of mucin gels. *Sci Adv* 2015;**1**:e1500501.
49. Gao W, Dong RF, Thamphiwatana S, Li JX, Gao WW, Zhang LF, et al. Artificial micromotors in the mouse's stomach: a step toward *in vivo* use of synthetic motors. *ACS Nano* 2015;**9**:117−23.
50. Zhang HY, Li ZS, Gao CY, Fan XJ, Pang YX, Li TL, et al. Dual-responsive biohybrid neutrobots for active target delivery. *Sci Robot* 2021;**6**:eaaz9519.
51. Medina-Sanchez M, Xu HF, Schmidt OG. Micro- and nano-motors: the new generation of drug carriers. *Ther Deliv* 2018;**9**:303−16.
52. Kagan D, Benchimol MJ, Claussen JC, Chuluun-Erdene E, Esener S, Wang J. Acoustic droplet vaporization and propulsion of perfluorocarbon-loaded microbullets for targeted tissue penetration and deformation. *Angew Chem Int Ed* 2012;**51**:7519−22.
53. Xi W, Solovev AA, Ananth AN, Gracias DH, Sanchez S, Schmidt OG. Rolled-up magnetic microdrillers: towards remotely controlled minimally invasive surgery. *Nanoscale* 2013;**5**:1294−7.
54. Wu ZG, Li L, Yang Y, Hu P, Li Y, Yang SY, et al. A microrobotic system guided by photoacoustic computed tomography for targeted navigation in intestines *in vivo*. *Sci Robot* 2019;**4**:eaax0613.
55. Sanchez S, Soler L, Katuri J. Chemically powered micro- and nanomotors. *Angew Chem Int Ed Engl* 2015;**54**:1414−44.
56. Ye YC, Luan JB, Wang M, Chen YM, Wilson DA, Peng F, et al. Fabrication of self-propelled micro- and nanomotors based on Janus structures. *Chemistry* 2019;**25**:8663−80.
57. Gibbs JG, Zhao YP. Self-organized multiconstituent catalytic nanomotors. *Small* 2010;**6**:1656−62.
58. Gibbs JG, Zhao YP. Design and characterization of rotational multicomponent catalytic nanomotors. *Small* 2009;**5**:2304−8.
59. Wang H, Pumera M. Fabrication of micro/nanoscale motors. *Chem Rev* 2015;**115**:8704−35.
60. Gao W, Feng XM, Pei A, Kane CR, Tam R, Hennessy C, et al. Bioinspired helical microswimmers based on vascular plants. *Nano Lett* 2014;**14**:305−10.
61. Wang Y, Mayorga-Martinez CC, Moo JGS, Pumera M. Structure-function dependence on template-based micromotors. *ACS Appl Energy Mater* 2018;**1**:3443−8.
62. Li JX, Li TL, Xu TL, Kiristi M, Liu WJ, Wu ZG, et al. Magneto-acoustic hybrid nanomotor. *Nano Lett* 2015;**15**:4814−21.
63. Loget G, Zigah D, Bouffier L, Sojic N, Kuhn A. Bipolar electrochemistry: from materials science to motion and beyond. *Acc Chem Res* 2013;**46**:2513−23.
64. Fattah Z, Garrigue P, Lapeyre V, Kuhn A, Bouffier L. Controlled orientation of asymmetric copper deposits on carbon microobjects by bipolar electrochemistry. *J Phys Chem C* 2012;**116**:22021−7.
65. Wilson DA, Nolte RJ, van Hest JC. Autonomous movement of platinum-loaded stomatocytes. *Nat Chem* 2012;**4**:268−74.
66. Wu YJ, Wu ZG, Lin XK, He Q, Li JB. Autonomous movement of controllable assembled Janus capsule motors. *ACS Nano* 2012;**6**:10910−6.
67. Abdelmohsen LK, Nijemeisland M, Pawar GM, Janssen GJ, Nolte RJ, van Hest JC, et al. Dynamic loading and unloading of proteins in polymeric stomatocytes: formation of an enzyme-loaded supramolecular nanomotor. *ACS Nano* 2016;**10**:2652−60.
68. Tu YF, Peng F, White PB, Wilson DA. Redox-sensitive stomatocyte nanomotors: destruction and drug release in the presence of glutathione. *Angew Chem Int Ed Engl* 2017;**56**:7620−4.
69. Tu YF, Peng F, Andre AAM, Men YJ, Srinivas M, Wilson DA. Biodegradable hybrid stomatocyte nanomotors for drug delivery. *ACS Nano* 2017;**11**:1957−63.
70. Wauters AC, Pijpers IAB, Mason AF, Williams DS, Tel J, Abdelmohsen L, et al. Development of morphologically discrete PEG-PDLLA nanotubes for precision nanomedicine. *Biomacromolecules* 2019;**20**:177−83.
71. Toebes BJ, Cao F, Wilson DA. Spatial control over catalyst positioning on biodegradable polymeric nanomotors. *Nat Commun* 2019;**10**:5308.
72. Ariga K, Hill JP, Ji QM. Layer-by-layer assembly as a versatile bottom-up nanofabrication technique for exploratory research and realistic application. *Phys Chem Chem Phys* 2007;**9**:2319−40.
73. Lin XK, Wu ZG, Wu YJ, Xuan MJ, He Q. Self-propelled micro-/nanomotors based on controlled assembled architectures. *Adv Mater* 2016;**28**:1060−72.
74. Zhang X, Chen H, Zhang HY. Layer-by-layer assembly: from conventional to unconventional methods. *Chem Commun* 2007:1395−405.
75. Wu ZG, Wu YJ, He WP, Lin XK, Sun JM, He Q. Self-propelled polymer-based multilayer nanorockets for transportation and drug release. *Angew Chem Int Ed Engl* 2013;**52**:7000−3.
76. Gao WL, Liu M, Liu LM, Zhang H, Dong B, Li CY. One-step fabrication of multifunctional micromotors. *Nanoscale* 2015;**7**:13918−23.
77. Sanchez S, Solovev AA, Mei YF, Schmidt OG. Dynamics of biocatalytic microengines mediated by variable friction control. *J Am Chem Soc* 2010;**132**:13144−5.
78. Yu WQ, Lin RY, He XQ, Yang XT, Zhang HL, Hu C, et al. Self-propelled nanomotor reconstructs tumor microenvironment through synergistic hypoxia alleviation and glycolysis inhibition for promoted anti-metastasis. *Acta Pharm Sin B* 2021;**11**:2924−36.
79. Magdanz V, Sanchez S, Schmidt OG. Development of a sperm-flagella driven micro-bio-robot. *Adv Mater* 2013;**25**:6581−8.
80. Stanton MM, Simmchen J, Ma X, Miguel-Lopez A, Sanchez S. Biohybrid Janus motors driven by *Escherichia coli*. *Adv Mater Interfaces* 2016;**3**:1500505.
81. Wu ZG, Li TL, Li JX, Gao W, Xu TL, Christianson C, et al. Turning erythrocytes into functional micromotors. *ACS Nano* 2014;**8**:12041−8.
82. Wan MM, Wang Q, Wang RL, Wu R, Li T, Fang D, et al. Platelet-derived porous nanomotor for thrombus therapy. *Sci Adv* 2020;**6**:eaaz9014.
83. Chen CR, Karshalev E, Li JX, Soto F, Castillo R, Campos I, et al. Transient micromotors that disappear when no longer needed. *ACS Nano* 2016;**10**:10389−96.
84. Chi QJ, Wang Z, Tian FF, You JA, Xu S. A review of fast bubble-driven micromotors powered by biocompatible fuel: low-concentration fuel, bioactive fluid and enzyme. *Micromachines* 2018;**9**:537.
85. Abdelmohsen L, Peng F, Tu YF, Wilson DA. Micro- and nano-motors for biomedical applications. *J Mater Chem B* 2014;**2**:2395−408.
86. Wang YM, Tu YF, Peng F. The energy conversion behind micro-and nanomotors. *Micromachines* 2021;**12**:222.
87. Sharma R, Chang ST, Velev OD. Gel-based self-propelling particles get programmed to dance. *Langmuir* 2012;**28**:10128−35.
88. Wang Y, Hernandez RM, Bartlett Jr DJ, Bingham JM, Kline TR, Sen A, et al. Bipolar electrochemical mechanism for the propulsion of catalytic nanomotors in hydrogen peroxide solutions. *Langmuir* 2006;**22**:10451−6.
89. Moran JL, Posner JD. Electrokinetic locomotion due to reaction-induced charge auto-electrophoresis. *J Fluid Mech* 2011;**680**:31−66.
90. Paxton WF, Sen A, Mallouk TE. Motility of catalytic nanoparticles through self-generated forces. *Chemistry* 2005;**11**:6462−70.
91. Jiang HR, Yoshinaga N, Sano M. Active motion of a Janus particle by self-thermophoresis in a defocused laser beam. *Phys Rev Lett* 2010;**105**:268302.
92. Dong RF, Cai YP, Yang YR, Gao W, Ren BY. Photocatalytic micro/nanomotors: from construction to applications. *Acc Chem Res* 2018;**51**:1940−7.
93. Villa K, Pumera M. Fuel-free light-driven micro/nanomachines: artificial active matter mimicking nature. *Chem Soc Rev* 2019;**48**:4966−78.
94. Moo JG, Presolski S, Pumera M. Photochromic spatiotemporal control of bubble-propelled micromotors by a spiropyran molecular switch. *ACS Nano* 2016;**10**:3543−52.
95. Hong YY, Diaz M, Cordova-Figueroa UM, Sen A. Light-driven titanium-dioxide-based reversible microfireworks and micromotor/micropump systems. *Adv Funct Mater* 2010;**20**:1568−76.

96. Wang ZB, Xu ZJ, Zhu B, Zhang Y, Lin JW, Wu YG, et al. Design, fabrication and application of magnetically actuated micro/-nanorobots: a review. *Nanotechnology* 2022;**33**:152001.
97. Zhang L, Abbott JJ, Dong LX, Peyer KE, Kratochvil BE, Zhang HX, et al. Characterizing the swimming properties of artificial bacterial flagella. *Nano Lett* 2009;**9**:3663−7.
98. Chen XZ, Hoop M, Mushtaq F, Siringil E, Hu CZ, Nelson BJ, et al. Recent developments in magnetically driven micro- and nanorobots. *Appl Mater Today* 2017;**9**:37−48.
99. Chang ST, Paunov VN, Petsev DN, Velev OD. Remotely powered self-propelling particles and micropumps based on miniature diodes. *Nat Mater* 2007;**6**:235−40.
100. Ni S, Marini E, Buttinoni I, Wolf H, Isa L. Hybrid colloidal microswimmers through sequential capillary assembly. *Soft Matter* 2017;**13**:4252−9.
101. Ahmed D, Baasch T, Jang B, Pane S, Dual J, Nelson BJ. Artificial swimmers propelled by acoustically activated flagella. *Nano Lett* 2016;**16**:4968−74.
102. Wang W, Zhou C. A journey of nanomotors for targeted cancer therapy: principles, challenges, and a critical review of the state-of-the-art. *Adv Healthc Mater* 2021;**10**:e2001236.
103. Ou JF, Liu K, Jiang JM, Wilson DA, Liu L, Wang F, et al. Micro-/nanomotors toward biomedical applications: the recent progress in biocompatibility. *Small* 2020;**16**:e1906184.
104. Peng F, Tu YF, van Hest JC, Wilson DA. Self-guided supramolecular cargo-loaded nanomotors with chemotactic behavior towards cells. *Angew Chem Int Ed Engl* 2015;**54**:11662−5.
105. Chalupniak A, Morales-Narvaez E, Merkoci A. Micro and nanomotors in diagnostics. *Adv Drug Deliv Rev* 2015;**95**:104−16.
106. Zhan XJ, Wang JZ, Xiong Z, Zhang X, Zhou Y, Zheng J, et al. Enhanced ion tolerance of electrokinetic locomotion in polyelectrolyte-coated microswimmer. *Nat Commun* 2019;**10**:3921.
107. Sridhar V, Podjaski F, Alapan Y, Kroger J, Grunenberg L, Kishore V, et al. Light-driven carbon nitride microswimmers with propulsion in biological and ionic media and responsive on-demand drug delivery. *Sci Robot* 2022;**7**:eabm1421.
108. Deng XY, Shao ZW, Zhao YL. Solutions to the drawbacks of photothermal and photodynamic cancer therapy. *Adv Sci* 2021;**8**:2002504.
109. Xie H, Sun MM, Fan XJ, Lin ZH, Chen WN, Wang L, et al. Reconfigurable magnetic microrobot swarm: multimode transformation, locomotion, and manipulation. *Sci Robot* 2019;**4**:eaav8006.
110. Li TL, Li JX, Morozov KI, Wu ZG, Xu TL, Rozen I, et al. Highly efficient freestyle magnetic nanoswimmer. *Nano Lett* 2017;**17**:5092−8.
111. Wang SH, Liu K, Zhou Q, Xu C, Gao JB, Wang Z, et al. Hydrogen-powered microswimmers for precise and active hydrogen therapy towards acute ischemic stroke. *Adv Funct Mater* 2021;**31**:2009475.
112. Wan MM, Chen H, Wang Q, Niu Q, Xu P, Yu YQ, et al. Bio-inspired nitric-oxide-driven nanomotor. *Nat Commun* 2019;**10**:966.
113. Wan MM, Liu ZY, Li T, Chen H, Wang Q, Chen TT, et al. Zwitterion-based hydrogen sulfide nanomotors induce multiple acidosis in tumor cells by destroying tumor metabolic symbiosis. *Angew Chem Int Ed Engl* 2021;**60**:16139−48.
114. Patino T, Arque X, Mestre R, Palacios L, Sanchez S. Fundamental aspects of enzyme-powered micro- and nanoswimmers. *Acc Chem Res* 2018;**51**:2662−71.
115. Dunderdale G, Ebbens S, Fairclough P, Howse J. Importance of particle tracking and calculating the mean-squared displacement in distinguishing nanopropulsion from other processes. *Langmuir* 2012;**28**:10997−1006.
116. Howse JR, Jones RA, Ryan AJ, Gough T, Vafabakhsh R, Golestanian R. Self-motile colloidal particles: from directed propulsion to random walk. *Phys Rev Lett* 2007;**99**:048102.
117. Wang W, Mallouk TE. A practical guide to analyzing and reporting the movement of nanoscale swimmers. *ACS Nano* 2021;**15**:15446−60.
118. Zhao X, Palacci H, Yadav V, Spiering MM, Gilson MK, Butler PJ, et al. Substrate-driven chemotactic assembly in an enzyme cascade. *Nat Chem* 2018;**10**:311−7.
119. Xu DD, Zhou C, Zhan C, Wang Y, You YQ, Pan X, et al. Enzymatic micromotors as a mobile photosensitizer platform for highly efficient on-chip targeted antibacteria photodynamic therapy. *Adv Funct Mater* 2019;**29**:1807727.
120. Wilson DA, de Nijs B, van Blaaderen A, Nolte RJ, van Hest JC. Fuel concentration dependent movement of supramolecular catalytic nanomotors. *Nanoscale* 2013;**5**:1315−8.
121. Xuan MJ, Mestre R, Gao CY, Zhou C, He Q, Sanchez S. Noncontinuous super-diffusive dynamics of a light-activated nanobottle motor. *Angew Chem Int Ed Engl* 2018;**57**:6838−42.
122. Ahmed D, Baasch T, Blondel N, Laubli N, Dual J, Nelson BJ. Neutrophil-inspired propulsion in a combined acoustic and magnetic field. *Nat Commun* 2017;**8**:770.
123. Chen CR, Mou FZ, Xu LL, Wang SF, Guan JG, Feng ZP, et al. Light-steered isotropic semiconductor micromotors. *Adv Mater* 2017;**29**:1603374.
124. Lin ZH, Fan XJ, Sun MM, Gao CY, He Q, Xie H. Magnetically actuated peanut colloid motors for cell manipulation and patterning. *ACS Nano* 2018;**12**:2539−45.
125. Baraban L, Harazim SM, Sanchez S, Schmidt OG. Chemotactic behavior of catalytic motors in microfluidic channels. *Angew Chem Int Ed Engl* 2013;**52**:5552−6.
126. Shao JX, Xuan MJ, Zhang HY, Lin XK, Wu ZG, He Q. Chemotaxis-guided hybrid neutrophil micromotors for targeted drug transport. *Angew Chem Int Ed Engl* 2017;**56**:12935−9.
127. Saha S, Golestanian R, Ramaswamy S. Clusters, asters, and collective oscillations in chemotactic colloids. *Phys Rev E Stat Nonlin Soft Matter Phys* 2014;**89**:062316.
128. Ji YX, Lin XK, Wu ZG, Wu YJ, Gao W, He Q. Macroscale chemotaxis from a swarm of bacteria-mimicking nanoswimmers. *Angew Chem Int Ed Engl* 2019;**58**:12200−5.
129. Zhou C, Gao CY, Wu YJ, Si TY, Yang MC, He Q. Torque-driven orientation motion of chemotactic colloidal motors. *Angew Chem Int Ed Engl* 2022;**61**:e202116013.
130. Dey KK, Bhandari S, Bandyopadhyay D, Basu S, Chattopadhyay A. The pH taxis of an intelligent catalytic microbot. *Small* 2013;**9**:1916−20.
131. Wang Y, Zhou C, Wang W, Xu DD, Zeng FY, Zhan C, et al. Photocatalytically powered matchlike nanomotor for light-guided active SERS sensing. *Angew Chem Int Ed Engl* 2018;**57**:13110−3.
132. Duan WT, Liu R, Sen A. Transition between collective behaviors of micromotors in response to different stimuli. *J Am Chem Soc* 2013;**135**:1280−3.
133. Mou FZ, Li XF, Xie Q, Zhang JH, Xiong K, Xu LL, et al. Active micromotor systems built from passive particles with biomimetic predator-prey interactions. *ACS Nano* 2020;**14**:406−14.
134. Yu JF, Jin DD, Chan KF, Wang QQ, Yuan K, Zhang L. Active generation and magnetic actuation of microrobotic swarms in bio-fluids. *Nat Commun* 2019;**10**:5631.
135. Liang X, Mou FZ, Huang Z, Zhang JH, You M, Xu LL, et al. Hierarchical microswarms with leader-follower-like structures: electrohydrodynamic self-organization and multimode collective photoresponses. *Adv Funct Mater* 2020;**30**:1908602.
136. Mou FM, Zhang JH, Wu Z, Du S, Zhang ZX, Xu LL, et al. Phototactic flocking of photochemical micromotors. *iScience* 2019;**19**:415−24.
137. Xu TL, Soto F, Gao W, Dong RF, Garcia-Gradilla V, Magana E, et al. Reversible swarming and separation of self-propelled chemically powered nanomotors under acoustic fields. *J Am Chem Soc* 2015;**137**:2163−6.
138. Yan J, Han M, Zhang J, Xu C, Luijten E, Granick S. Reconfiguring active particles by electrostatic imbalance. *Nat Mater* 2016;**15**:1095−9.
139. Yu JF, Wang B, Du XZ, Wang QQ, Zhang L. Ultra-extensible ribbon-like magnetic microswarm. *Nat Commun* 2018;**9**:3260.

140. Zhou DK, Gao Y, Yang JJ, Li YC, Shao GB, Zhang GY, et al. Light-ultrasound driven collective "Firework" behavior of nanomotors. *Adv Sci* 2018;**5**:1800122.
141. Bergeles C, Kratochvil BE, Nelson BJ. Visually servoing magnetic intraocular microdevices. *IEEE Trans Robot* 2012;**28**:798−809.
142. Ullrich F, Bergeles C, Pokki J, Ergeneman O, Erni S, Chatzipirpiridis G, et al. Mobility experiments with microrobots for minimally invasive intraocular surgery. *Invest Ophthalmol Vis Sci* 2013;**54**:2853−63.
143. Huang D, Swanson EA, Lin CP, Schuman JS, Stinson WG, Chang W, et al. Optical coherence tomography. *Science* 1991;**254**:1178−81.
144. Aziz A, Pane S, Iacovacci V, Koukourakis N, Czarske J, Menciassi A, et al. Medical imaging of microrobots: toward *in vivo* applications. *ACS Nano* 2020;**14**:10865−93.
145. Li DF, Dong DR, Lam WS, Xing LX, Wei TY, Sun D. Automated *in vivo* navigation of magnetic-driven microrobots using OCT imaging feedback. *IEEE Trans Biomed Eng* 2020;**67**:2349−58.
146. Servant A, Qiu FM, Mazza M, Kostarelos K, Nelson BJ. Controlled *in vivo* swimming of a swarm of bacteria-like microrobotic flagella. *Adv Mater* 2015;**27**:2981−8.
147. Yan XH, Zhou Q, Vincent M, Deng Y, Yu JF, Xu JB, et al. Multifunctional biohybrid magnetite microrobots for imaging-guided therapy. *Sci Robot* 2017;**2**:eaaq1155.
148. Wang B, Chan KF, Yuan K, Wang Q, Xia X, Yang L, et al. Endoscopy-assisted magnetic navigation of biohybrid soft microrobots with rapid endoluminal delivery and imaging. *Sci Robot* 2021;**6**:eabd2813.
149. Yu JF, Wang QQ, Li MZ, Liu C, Wang LD, Xu TT, et al. Characterizing nanoparticle swarms with tuneable concentrations for enhanced imaging contrast. *IEEE Robot Autom Lett* 2019;**4**:2942−9.
150. Singh AV, Dad Ansari MH, Dayan CB, Giltinan J, Wang S, Yu Y, et al. Multifunctional magnetic hairbot for untethered osteogenesis, ultrasound contrast imaging and drug delivery. *Biomaterials* 2019;**219**:119394.
151. Benoit MR, Mayer D, Barak Y, Chen IY, Hu W, Cheng Z, et al. Visualizing implanted tumors in mice with magnetic resonance imaging using magnetotactic bacteria. *Clin Cancer Res* 2009;**15**:5170−7.
152. Nothnagel N, Rahmer J, Gleich B, Halkola A, Buzug TM, Borgert J. Steering of magnetic devices with a magnetic particle imaging system. *IEEE Trans Biomed Eng* 2016;**63**:2286−93.
153. Griese F, Knopp T, Gruettner C, Thieben F, Muller K, Loges S, et al. Simultaneous magnetic particle imaging and navigation of large superparamagnetic nanoparticles in bifurcation flow experiments. *J Magn Magn Mater* 2020;**498**:166206.
154. Bakenecker AC, von Gladiss A, Friedrich T, Heinen U, Lehr H, Ludtke-Buzug K, et al. Actuation and visualization of a magnetically coated swimmer with magnetic particle imaging. *J Magn Magn Mater* 2019;**473**:495−500.
155. Zhao JH, Chen JW, Ma SN, Liu QQ, Huang LX, Chen XN, et al. Recent developments in multimodality fluorescence imaging probes. *Acta Pharm Sin B* 2018;**8**:320−38.
156. Nguyen PB, Kang B, Bappy DM, Choi E, Park S, Ko SY, et al. Real-time microrobot posture recognition *via* biplane X-ray imaging system for external electromagnetic actuation. *Int J Comput Assist Radiol Surg* 2018;**13**:1843−52.
157. Jeong S, Choi H, Go G, Lee C, Lim KS, Sim DS, et al. Penetration of an artificial arterial thromboembolism in a live animal using an intravascular therapeutic microrobot system. *Med Eng Phys* 2016;**38**:403−10.
158. Vilela D, Cossio U, Parmar J, Martinez-Villacorta AM, Gomez-Vallejo V, Llop J, et al. Medical imaging for the tracking of micromotors. *ACS Nano* 2018;**12**:1220−7.
159. Iacovacci V, Blanc A, Huang HW, Ricotti L, Schibli R, Menciassi A, et al. High-resolution SPECT imaging of stimuli-responsive soft microrobots. *Small* 2019;**15**:e1900709.
160. Aziz A, Medina-Sanchez M, Claussen J, Schmidt OG. Real-time optoacoustic tracking of single moving micro-objects in deep phantom and *ex vivo* tissues. *Nano Lett* 2019;**19**:6612−20.
161. Xie LS, Pang X, Yan XH, Dai QX, Lin HR, Ye J, et al. Photoacoustic imaging-trackable magnetic microswimmers for pathogenic bacterial infection treatment. *ACS Nano* 2020;**14**:2880−93.
162. Xu DD, Hu J, Pan X, Sanchez S, Yan XH, Ma X. Enzyme-powered liquid metal nanobots endowed with multiple biomedical functions. *ACS Nano* 2021;**15**:11543−54.
163. Zhong DN, Li WL, Qi YC, He J, Zhou M. Photosynthetic biohybrid nanoswimmers system to alleviate tumor hypoxia for FL/PA/MR imaging-guided enhanced radio-photodynamic synergetic therapy. *Adv Funct Mater* 2020;**30**:1910395.
164. Tooke JE, Milligan DW. Capillary flow velocity in leukaemia. *Br Med J* 1983;**286**:518−9.
165. Alapan Y, Bozuyuk U, Erkoc P, Karacakol AC, Sitti M. Multifunctional surface microrollers for targeted cargo delivery in physiological blood flow. *Sci Robot* 2020;**5**:eaba5726.
166. Wang QQ, Chan KF, Schweizer K, Du XZ, Jin DD, Yu SCH, et al. Ultrasound Doppler-guided real-time navigation of a magnetic microswarm for active endovascular delivery. *Sci Adv* 2021;**7**:eabe5914.
167. Pardridge WM. Blood−brain barrier delivery. *Drug Discov Today* 2007;**12**:54−61.
168. Han L, Jiang C. Evolution of blood−brain barrier in brain diseases and related systemic nanoscale brain-targeting drug delivery strategies. *Acta Pharm Sin B* 2021;**11**:2306−25.
169. Joseph A, Contini C, Cecchin D, Nyberg S, Ruiz-Perez L, Gaitzsch J, et al. Chemotactic synthetic vesicles: design and applications in blood−brain barrier crossing. *Sci Adv* 2017;**3**:e1700362.
170. Somasundar A, Sen A. Chemically propelled nano and micromotors in the body: quo vadis?. *Small* 2021;**17**:e2007102.
171. Liu HJ, Wen J, Xiao Y, Liu J, Hopyan S, Radisic M, et al. *In situ* mechanical characterization of the cell nucleus by atomic force microscopy. *ACS Nano* 2014;**8**:3821−8.
172. Xuan MJ, Shao JX, Gao CY, Wang W, Dai LR, He Q. Self-propelled nanomotors for thermomechanically percolating cell membranes. *Angew Chem Int Ed Engl* 2018;**57**:12463−7.
173. Wang W, Wu ZG, Lin XK, Si TY, He Q. Gold-nanoshell-functionalized polymer nanoswimmer for photomechanical poration of single-cell membrane. *J Am Chem Soc* 2019;**141**:6601−8.
174. Ma EH, Wang K, Wang H. An immunoassay based on nanomotor-assisted electrochemical response for the detection of immunoglobulin. *Mikrochim Acta* 2022;**189**:47.
175. Beltran-Gastelum M, Esteban-Fernandez de Avila B, Gong H, Venugopalan PL, Hianik T, Wang J, et al. Rapid detection of AIB1 in breast cancer cells based on aptamer-functionalized nanomotors. *ChemPhysChem* 2019;**20**:3177−80.
176. Mayorga-Martinez CC, Pumera M. Self-propelled tags for protein detection. *Adv Funct Mater* 2020;**30**:1906449.
177. de Avila BE, Zhao MJ, Campuzano S, Ricci F, Pingarron JM, Mascini M, et al. Rapid micromotor-based naked-eye immunoassay. *Talanta* 2017;**167**:651−7.
178. Wang Y, Liu XX, Chen C, Chen YD, Li Y, Ye H, et al. Magnetic nanorobots as maneuverable immunoassay probes for automated and efficient enzyme linked immunosorbent assay. *ACS Nano* 2022;**16**:180−91.
179. Russell SM, Alba-Patino A, Borges M, de la Rica R. Multifunctional motion-to-color janus transducers for the rapid detection of sepsis biomarkers in whole blood. *Biosens Bioelectron* 2019;**140**:111346.
180. Xie YZ, Fu SZ, Wu J, Lei JP, Ju HX. Motor-based microprobe powered by bio-assembled catalase for motion detection of DNA. *Biosens Bioelectron* 2017;**87**:31−7.
181. Fu SZ, Zhang XQ, Xie YZ, Wu J, Ju HX. An efficient enzyme-powered micromotor device fabricated by cyclic alternate hybridization assembly for DNA detection. *Nanoscale* 2017;**9**:9026−33.
182. Zhang XQ, Chen CT, Wu J, Ju HX. Bubble-propelled jellyfish-like micromotors for DNA sensing. *ACS Appl Mater Interfaces* 2019;**11**:13581−8.
183. Esteban-Fernandez de Avila B, Martin A, Soto F, Lopez-Ramirez MA, Campuzano S, Vasquez-Machado GM, et al. Single cell real-time miRNAs sensing based on nanomotors. *ACS Nano* 2015;**9**:6756−64.

184. Jurado-Sanchez B, Pacheco M, Rojo J, Escarpa A. Magnetocatalytic graphene quantum dots Janus micromotors for bacterial endotoxin detection. *Angew Chem Int Ed Engl* 2017;**56**:6957−61.
185. Zhang YB, Zhang L, Yang LD, Vong CI, Chan KF, Wu WKK, et al. Real-time tracking of fluorescent magnetic spore-based microrobots for remote detection of *C. diff* toxins. *Sci Adv* 2019;**5**:eaau9650.
186. Patino T, Porchetta A, Jannasch A, Llado A, Stumpp T, Schaffer E, et al. Self-sensing enzyme-powered micromotors equipped with pH-responsive DNA nanoswitches. *Nano Lett* 2019;**19**:3440−7.
187. Leong TG, Randall CL, Benson BR, Bassik N, Stern GM, Gracias DH. Tetherless thermobiochemically actuated microgrippers. *Proc Natl Acad Sci U S A* 2009;**106**:703−8.
188. Bassik N, Brafman A, Zarafshar AM, Jamal M, Luvsanjav D, Selaru FM, et al. Enzymatically triggered actuation of miniaturized tools. *J Am Chem Soc* 2010;**132**:16314−7.
189. Gultepe E, Yamanaka S, Laflin KE, Kadam S, Shim Y, Olaru AV, et al. Biologic tissue sampling with untethered microgrippers. *Gastroenterology* 2013;**144**:691−3.
190. Wang Y, Liu YH, Li Y, Xu DD, Pan X, Chen YD, et al. Magnetic nanomotor-based maneuverable SERS probe. *Research* 2020;**2020**:7962024.
191. Zhao L, Liu Y, Xie SZ, Ran P, Wei JJ, Liu QJ, et al. Janus micromotors for motion-capture-ratiometric fluorescence detection of circulating tumor cells. *Chem Eng J* 2020;**382**:123041.
192. Olson ES, Orozco J, Wu Z, Malone CD, Yi B, Gao W, et al. Toward *in vivo* detection of hydrogen peroxide with ultrasound molecular imaging. *Biomaterials* 2013;**34**:8918−24.
193. Steiner MS, Duerkop A, Wolfbeis OS. Optical methods for sensing glucose. *Chem Soc Rev* 2011;**40**:4805−39.
194. Campuzano S, Orozco J, Kagan D, Guix M, Gao W, Sattayasamitsathit S, et al. Bacterial isolation by lectin-modified microengines. *Nano Lett* 2012;**12**:396−401.
195. Draz MS, Lakshminaraasimulu NK, Krishnakumar S, Battalapalli D, Vasan A, Kanakasabapathy MK, et al. Motion-based immunological detection of Zika virus using Pt-nanomotors and a cellphone. *ACS Nano* 2018;**12**:5709−18.
196. Zheng SH, Wang Y, Pan SH, Ma EH, Jin S, Jiao M, et al. Biocompatible nanomotors as active diagnostic imaging agents for enhanced magnetic resonance imaging of tumor tissues *in vivo*. *Adv Funct Mater* 2021;**31**:2100936.
197. Feng YW, Chang XC, Liu H, Hu Y, Li TL, Li LQ. Multi-response biocompatible Janus micromotor for ultrasonic imaging contrast enhancement. *Appl Mater Today* 2021;**23**:101026.
198. St John A, Caturegli I, Kubicki NS, Kavic SM. The rise of minimally invasive surgery: 16 year analysis of the progressive replacement of open surgery with laparoscopy. *J Soc Laparoendosc Surg* 2020;**24**.e2020.00076.
199. Soto F, Wang J, Ahmed R, Demirci U. Medical micro/nanorobots in precision medicine. *Adv Sci* 2020;**7**:2002203.
200. Solovev AA, Xi W, Gracias DH, Harazim SM, Deneke C, Sanchez S, et al. Self-propelled nanotools. *ACS Nano* 2012;**6**:1751−6.
201. Jin QR, Yang YQ, Jackson JA, Yoon C, Gracias DH. Untethered single cell grippers for active biopsy. *Nano Lett* 2020;**20**:5383−90.
202. Chatzipirpiridis G, Ergeneman O, Pokki J, Ullrich F, Fusco S, Ortega JA, et al. Electroforming of implantable tubular magnetic microrobots for wireless ophthalmologic applications. *Adv Healthc Mater* 2015;**4**:209−14.
203. Gultepe E, Randhawa JS, Kadam S, Yamanaka S, Selaru FM, Shin EJ, et al. Biopsy with thermally-responsive untethered microtools. *Adv Mater* 2013;**25**:514−9.
204. Singh AV, Sitti M. Targeted drug delivery and imaging using mobile milli/microrobots: a promising future towards theranostic pharmaceutical design. *Curr Pharm Des* 2016;**22**:1418−28.
205. Yang R, Wei T, Goldberg H, Wang WP, Cullion K, Kohane DS. Getting drugs across biological barriers. *Adv Mater* 2017;**29**:1606596.
206. Lin RY, Yu WQ, Chen XC, Gao HL. Self-propelled micro/-nanomotors for tumor targeting delivery and therapy. *Adv Healthc Mater* 2021;**10**:e2001212.
207. Esteban-Fernandez de Avila B, Angell C, Soto F, Lopez-Ramirez MA, Baez DF, Xie SB, et al. Acoustically propelled nanomotors for intracellular siRNA delivery. *ACS Nano* 2016;**10**:4997−5005.
208. Hortelao AC, Patino T, Perez-Jimenez A, Blanco A, Sanchez S. Enzyme-powered nanobots enhance anticancer drug delivery. *Adv Funct Mater* 2018;**28**:1705086.
209. Medina-Sanchez M, Schwarz L, Meyer AK, Hebenstreit F, Schmidt OG. Cellular cargo delivery: toward assisted fertilization by sperm-carrying micromotors. *Nano Lett* 2016;**16**:555−61.
210. Wu BY, Fu JT, Zhou YX, Luo SL, Zhao YT, Quan GL, et al. Tailored core-shell dual metal-organic frameworks as a versatile nanomotor for effective synergistic antitumor therapy. *Acta Pharm Sin B* 2020;**10**:2198−211.
211. Li JX, Thamphiwatana S, Liu WJ, Esteban-Fernandez de Avila B, Angsantikul P, Sandraz E, et al. Enteric micromotor can selectively position and spontaneously propel in the gastrointestinal tract. *ACS Nano* 2016;**10**:9536−42.
212. de Avila BE, Angsantikul P, Li JX, Angel Lopez-Ramirez M, Ramirez-Herrera DE, Thamphiwatana S, et al. Micromotor-enabled active drug delivery for *in vivo* treatment of stomach infection. *Nat Commun* 2017;**8**:272.
213. Li JX, Angsantikul P, Liu WJ, Esteban-Fernandez de Avila B, Thamphiwatana S, Xu ML, et al. Micromotors spontaneously neutralize gastric acid for pH-responsive payload release. *Angew Chem Int Ed Engl* 2017;**56**:2156−61.
214. Wei XL, Beltran-Gastelum M, Karshalev E, Esteban-Fernandez de Avila B, Zhou JR, Ran DN, et al. Biomimetic micromotor enables active delivery of antigens for oral vaccination. *Nano Lett* 2019;**19**:1914−21.
215. Wu ZY, Wu R, Li XY, Wang XW, Tang XT, Tan KY, et al. Multi-pathway microenvironment regulation for atherosclerosis therapy based on beta-cyclodextrin/L-arginine/Au nanomotors with dual-mode propulsion. *Small* 2022;**18**:e2104120.
216. Wang C, Fernandez de Avila BE, Mundaca-Uribe R, Lopez-Ramirez MA, Ramirez-Herrera DE, Shukla S, et al. Active delivery of VLPs promotes anti-tumor activity in a mouse ovarian tumor model. *Small* 2020;**16**:e1907150.
217. Guo Q, Jiang C. Delivery strategies for macromolecular drugs in cancer therapy. *Acta Pharm Sin B* 2020;**10**:979−86.
218. Ye YC, Tong F, Wang SH, Jiang JM, Gao JB, Liu L, et al. Apoptotic tumor DNA activated nanomotor chemotaxis. *Nano Lett* 2021;**21**:8086−94.
219. Chen H, Shi T, Wang Y, Liu ZY, Liu FC, Zhang HY, et al. Deep penetration of nanolevel drugs and micrometer-level T cells promoted by nanomotors for cancer immunochemotherapy. *J Am Chem Soc* 2021;**143**:12025−37.
220. Li SP, Jiang Q, Liu SL, Zhang YL, Tian YH, Song C, et al. A DNA nanorobot functions as a cancer therapeutic in response to a molecular trigger *in vivo*. *Nat Biotechnol* 2018;**36**:258−64.
221. Deng GJ, Peng XH, Sun ZH, Zheng W, Yu J, Du LL, et al. Natural-killer-cell-inspired nanorobots with aggregation-induced emission characteristics for near-infrared-II fluorescence-guided glioma theranostics. *ACS Nano* 2020;**14**:11452−62.